Thermal and structural properties of the liquid-vapor interface in dipolar fluids

Peter Frodl and S. Dietrich
Fachbereich Physik, Bergische Universität Wuppertal, Postfach 100127, D-42097 Wuppertal, Federal Republic of Germany
(Received 21 April 1993)

Based on a recently developed density-functional theory for inhomogeneous molecular fluids [P. Frodl and S. Dietrich, Phys. Rev. A **45**, 7330 (1992)], we investigate the profiles of the number density and of the orientational order at the liquid-vapor interface of a Stockmayer fluid as well as the corresponding surface tension. We systematically analyze the dependencies of these quantities on the temperature and on the strength of the permanent dipole moment of the molecules. This reveals power laws and scaling behavior. Our approach, which is reliable even for large dipole moments, allows us to determine separately those contributions to the surface tension which are due to the orientational degrees of freedom.

PACS number(s): 61.25.Em, 64.70.Fx, 68.10.Cr, 82.65.Dp

I. INTRODUCTION

Under suitable conditions for pressure and temperature, the interface between a vapor phase g and the solid wall w confining it can be wetted by the corresponding liquid phase l. This means that the structure of the wall-vapor interface undergoes a phase transition such that it splits into the wall-liquid and the liquid-vapor interfaces separated by a macroscopically thick liquid film. There have been numerous efforts to understand this kind of interfacial phase transition on the basis of statistical mechanics [1–3]. Most of these theoretical studies are based on models which assume spherical molecules interacting with spherically symmetric pair potentials of the Lennard-Jones type. On the other hand, to a large extent the corresponding experiments are performed by using fluids whose particles carry a permanent dipole moment $\mathbf{m}$ which gives rise to the anisotropic and even-longer-ranged dipole-dipole interaction potential. Since the *range* of the interactions has turned out to be particularly important for the correct description of wetting phenomena, the aforementioned theoretical models thus appear to be still too crude for an accurate description of numerous actual experiments.

In order to narrow this gap between theory and experiment we recently developed a density-functional theory for inhomogeneous molecular fluids which is capable of describing wetting phenomena of one-component Stockmayer fluids. These are characterized by a pair interaction potential which is the sum of an isotropic Lennard-Jones potential and of the anisotropic dipole-dipole interaction between the permanent dipoles. Compared with previous theories of that kind our approach has the virtue to be reliable even for strong dipole moments. For this advantage one has to pay the price of substantially increased technical efforts whose details are expounded in Ref. [4].

In order to carry out the aforementioned program of understanding the splitting of the $w|g$ interface into the $w|l$ and the $l|g$ interfaces one must study the various ingredients by one and the same theory: (i) The bulk properties of this model have been analyzed in detail in Ref. [4] and their status with respect to simulations and other theoretical approaches has been assessed. We were able to conclude that our method yields quantitatively reliable results for the bulk. (ii) As the second ingredient it is the purpose of the present paper to analyze the thermal and structural properties of the free intrinsic liquid-vapor interface. Whereas the general analytic formulas for the number density profiles, the profiles of the orientational order, and the surface tension have been derived in Ref. [4], here we present the results obtained from their numerical evaluation. (iii) and (iv) The studies of the $w|l$ and finally of the $w|g$ interface will follow later.

We want to emphasize that the analysis of the free liquid-vapor interface of molecular fluids is not only relevant as an ingredient for wetting phenomena but it is interesting on its own both theoretically and experimentally. For a full account of the present state of the corresponding literature and for a critical comparison between our approach and others the reader is referred to Ref. [4].

The paper is organized such that in Sec. II we define our model and provide the basic analytic formulas. In Sec. III we present the numerical results for the number density profiles and for the profiles of the orientational order whereas Sec. IV is devoted to the surface tension. Section V contains a detailed discussion of our results and a critical comparison with the literature. We summarize our results in Sec. VI. Certain technical details which are important for obtaining reliable numerical results are given in Appendixes A, B, and C.

II. DENSITY-FUNCTIONAL THEORY FOR STOCKMAYER FLUIDS

In a one-component inhomogeneous and anisotropic fluid, $\hat{\rho}(\mathbf{r},\omega)$ denotes the number density of particles at the point $\mathbf{r}=(x,y,z)$ which have an orientation $\omega=(\theta,\phi)$ with respect to the space fixed coordinate system (see Fig. 1 in Ref. [4]). The total number density of particles without specified orientation is given by

$$\rho(\mathbf{r})=\int d\omega\,\hat{\rho}(\mathbf{r},\omega)=\int_0^{2\pi}d\phi\int_0^{\pi}d\theta(\sin\theta)\hat{\rho}(\mathbf{r},\theta,\phi)\ . \tag{2.1}$$

This allows us to split $\hat{\rho}$ into the total number density ρ and a normalized space- and angle-dependent factor α:

$$\hat{\rho}(\mathbf{r},\omega)=\rho(\mathbf{r})\alpha(\mathbf{r},\omega) , \quad \int d\omega\, \alpha(\mathbf{r},\omega)=1 . \tag{2.2}$$

The Stockmayer fluid, on which we focus, consists of spherically shaped molecules interacting via a Lennard-Jones potential,

$$w_{\mathrm{LJ}}(r_{12})=4\varepsilon\left[\left[\frac{\sigma}{r_{12}}\right]^{12}-\left[\frac{\sigma}{r_{12}}\right]^{6}\right] , \tag{2.3}$$

to which an interaction is added due to point dipoles embedded in spheres of diameter σ:

$$w_{\mathrm{dip}}(\mathbf{r},\mathbf{r}',\omega,\omega')=w_{\mathrm{dip}}(\mathbf{r}_{12}=\mathbf{r}-\mathbf{r}',\omega,\omega')$$
$$=\begin{cases}0 , & r_{12}\le\sigma \\ -\dfrac{m^2}{r_{12}^3}\left[\dfrac{3[\hat{\mathbf{m}}(\omega)\cdot\mathbf{r}_{12}][\hat{\mathbf{m}}(\omega')\cdot\mathbf{r}_{12}]}{r_{12}^2}-\hat{\mathbf{m}}(\omega)\cdot\hat{\mathbf{m}}(\omega')\right] , & r_{12}>\sigma .\end{cases} \tag{2.4}$$

m is the absolute value of the dipole moment and $\hat{\mathbf{m}}(\omega)$ is its unit vector. Thus the total pair potential is given by

$$w(\mathbf{r},\mathbf{r}',\omega,\omega')=w_{\mathrm{LJ}}(r_{12})+w_{\mathrm{dip}}(\mathbf{r},\mathbf{r}',\omega,\omega') . \tag{2.5}$$

By using the bulk pair distribution function in its low-density limit and by choosing the decomposition of w into a repulsive and an attractive part due to Barker and Henderson, one obtains in the absence of external fields the following approximate expression for the grand-canonical variational potential (see Ref. [4]):

$$\Omega[\{\hat{\rho}(\mathbf{r},\omega)\},T,\mu]=\mathcal{F}_{\mathrm{ref}}[\{\hat{\rho}(\mathbf{r},\omega)\},T]+\frac{1}{2\beta}\int\int d^3r\, d^3r' d\omega\, d\omega' \rho(\mathbf{r})\rho(\mathbf{r}')\alpha(\mathbf{r},\omega)\alpha(\mathbf{r}',\omega')e^{-\beta\omega_{\mathrm{ref}}(\mathbf{r},\mathbf{r}')}(1-e^{-\beta\omega_{\mathrm{ex}}(\mathbf{r},\mathbf{r}',\omega,\omega')})$$
$$-\mu\int d^3r\, d\omega\, \rho(\mathbf{r})\alpha(\mathbf{r},\omega)+\int d^3r\, \kappa(\mathbf{r})\left[1-\int d\omega\, \alpha(\mathbf{r},\omega)\right] ; \tag{2.6}$$

μ is the chemical potential, T denotes the temperature with $\beta=(k_B T)^{-1}$, $w_{\mathrm{ref}}(r_{12})=\Theta(\sigma-r_{12})w_{\mathrm{LJ}}(r_{12})$, $\Theta(x)$ is the Heaviside step function, and the excess interaction is given by

$$w_{\mathrm{ex}}(\mathbf{r},\mathbf{r}',\omega,\omega')=\Theta(r_{12}-\sigma)w(\mathbf{r},\mathbf{r}',\omega,\omega') . \tag{2.7}$$

The Helmholtz free energy of the reference system has the form

$$\mathcal{F}_{\mathrm{ref}}[\{\hat{\rho}(\mathbf{r},\omega)\},T]$$
$$=\int d^3r\, f_{\mathrm{ref}}^{\mathrm{HS}}(\rho(\mathbf{r}),T)$$
$$+\frac{1}{\beta}\int d^3r\int d\omega\, \alpha(\mathbf{r},\omega)\ln[4\pi\alpha(\mathbf{r},\omega)] \tag{2.8}$$

with the free energy density due to Carnahan and Starling [5]

$$f_{\mathrm{ref}}^{\mathrm{HS}}(\rho,T)=\frac{\rho}{\beta}\left[\ln(\rho\lambda^3)-1+\frac{4\eta-3\eta^2}{(1-\eta)^2}\right] , \tag{2.9}$$

where λ is the thermal de Broglie wavelength and $\eta=(\pi/6)d^3\rho$ denotes the packing fraction with a temperature-dependent hard-sphere diameter as given by Barker and Henderson [6]

$$d(T)=\int_0^\infty dr(1-e^{-\beta w_{\mathrm{ref}}(r)}) . \tag{2.10}$$

The last term in Eq. (2.8) is the extra contribution to the entropy of the reference system due to the fact that, even without dipolar interactions in the reference system, the corresponding structureless hard spheres HS are tagged by their embedded dipole moments. It vanishes in the case of an isotropic distribution $\alpha(\mathbf{r},\omega)=1/4\pi$. Equation (2.10) mimics the actually soft repulsive part of the Lennard-Jones intermolecular potential. In Eq. (2.6) the equilibrium value of the Lagrange parameter $\kappa(\mathbf{r},T,\mu)$ follows from the normalization condition for the orientational distribution [see Eq. (2.2)].

The actual grand-canonical free energy is the minimum of the variational functional and determines the equilibrium density configuration:

$$\Omega(T,\mu)=\min_{\hat{\rho}(\mathbf{r},\omega)}\Omega[\{\hat{\rho}(\mathbf{r},\omega)\},T,\mu]$$
$$=\Omega[\{\hat{\rho}_{\mathrm{eq}}(\mathbf{r},\omega;T,\mu)\},T,\mu] , \tag{2.11}$$

obtained by

$$\left.\frac{\delta\Omega[\{\hat{\rho}(\mathbf{r},\omega)\},T,\mu]}{\delta\hat{\rho}(\mathbf{r},\omega)}\right|_{\hat{\rho}(\mathbf{r},\omega)=\hat{\rho}_{\mathrm{eq}}(\mathbf{r},\omega;T,\mu)}=0 . \tag{2.12}$$

The properties of the homogeneous and isotropic bulk phases, i.e., $\rho(\mathbf{r})=\mathrm{const}$ and $\alpha(\mathbf{r},\omega)=1/4\pi$, as well as the bulk phase diagrams predicted by Eq. (2.6) are discussed in Sec. III and Appendix A of Ref. [4], respectively. The knowledge of the bulk phase diagrams enables us to choose the chemical potential $\mu=\mu_0(T)$ such that, for a given temperature, the liquid and vapor phases coexist. For that choice of the thermodynamic variables we can

impose vertical boundary conditions such that for $z \to +\infty$ one encounters the vapor phase and for $z \to -\infty$ the liquid phase. The lateral boundary conditions are chosen such that the mean position of the resulting interface of area A is fixed in the plane $z=0$. (For a discussion of the mean position of the free liquid-gas interface, see Ref. [7].) The system is translationally invariant in the x and y directions. Under these circumstances the total number density $\rho(\mathbf{r})$ is a function of z and the orientational profile $\alpha(\mathbf{r},\omega)=\alpha(z,\theta)=\bar{\alpha}(z,\theta)/(2\pi)$ depends only on z and the angle θ between the z axis and the dipole moment $\mathbf{m}$ of a particle (see Fig. 1 in Ref. [4]). The angular dependence of α can be expressed in terms of Legendre polynomials $\mathcal{P}_l$:

$$\bar{\alpha}(z,\theta)=\sum_{l=0}^{\infty}\alpha_l(z)\mathcal{P}_l(\cos\theta) = \frac{1}{2}+\frac{3\cos^2\theta-1}{2}\alpha_2(z)+\cdots . \tag{2.13}$$

Due to the normalization of $\alpha(\mathbf{r},\omega)$ [see Eq. (2.2)] $\alpha_0(z)=\frac{1}{2}$. In the absence of external fields $\alpha_l(z)=0$ for odd values of l [4]. Since $\alpha_2(z)$ provides the major contribution to the anisotropic orientation of the dipolar particles at the liquid-vapor interface [8] we constrain our analysis to terms up to second order in the Legendre polynomials [see Eq. (2.13) and Ref. [4]]. Since the coexisting liquid (l) and vapor (g) phases in the bulk are isotropic, one has the following boundary conditions for the liquid-vapor interface:

$$\rho(z\to-\infty)=\rho_l\ ,\quad \rho(z\to+\infty)=\rho_g\ , \qquad \alpha_2(z\to-\infty)=0\ ,\quad \alpha_2(z\to+\infty)=0\ . \tag{2.14}$$

Together with Eq. (2.13) the minimization of the variational grand-canonical functional [see Eq. (2.12)] leads to the following closed set of integral equations for the two unknown functions $\rho(z)$ and $\alpha_2(z)$ [see Eqs. (4.25) and (4.26) in Ref. [4]]:

$$\mu_{\mathrm{HS}}(z)=\mu_0(T)-\left[p_0(z)-\frac{1}{2}p_2(z) -\frac{1}{\beta}\ln\int_0^1 dx\, e^{-(3/2)\beta p_2(z)x^2}\right], \tag{2.15}$$

$$\alpha_2(z)=\frac{5}{4}\left[\frac{3\int_0^1 dx\, x^2 e^{-(3/2)\beta p_2(z)x^2}}{\int_0^1 dx e^{-(3/2)\beta p_2(z)x^2}}-1\right]. \tag{2.16}$$

$\mu_{\mathrm{HS}}(z)$ is the local chemical potential of the reference system:

$$\mu_{\mathrm{HS}}(z)=\left.\frac{\partial f_{\mathrm{ref}}^{\mathrm{HS}}(\rho,T)}{\partial\rho}\right|_{\rho=\rho(z)}=\mu_{\mathrm{HS}}[\rho(z)]\ . \tag{2.17}$$

The coefficients $p_0(z)$ and $p_2(z)$ are functionals of $\rho(z)$ and $\alpha_2(z)$:

$$p_m(z)=-\frac{\pi}{\beta}\int_{-\infty}^{\infty}dz'\rho(z')[w_{m0}(z'-z) +\alpha_2(z')w_{m2}(z'-z)]\ , \qquad m=0,2\ . \tag{2.18}$$

The functions w_{mn} are determined by the interaction potential w [see Eq. (2.5)] and the temperature. Their explicit but lengthy integral representations are presented in Appendix A where we also discuss their analytic properties [see Eqs. (A22)–(A25)]. Based on these expressions as well as on Eqs. (2.9), (2.10), (2.17), and (2.18), the equilibrium number density profiles $\rho_{\mathrm{eq}}(z;T)$ and orientational order profiles $\alpha_2^{\mathrm{eq}}(z;T)$ follow from solving Eqs. (2.15) and (2.16) numerically. [For a more explicit presentation see Eqs. (A27)–(A31); important details of the numerical technique we used are presented in Appendix B.]

III. PROFILES OF THE NUMBER DENSITY AND OF THE ORIENTATIONAL ORDER

In this section we present a systematic analysis of the dependence of $\rho(z)$ and $\alpha_2(z)$ on the temperature T and the strength m of the permanent dipoles. (Here and in the following we suppress the index eq.) This analysis is based on the numerical solutions of Eqs. (2.15) and (2.16) (see also Appendixes A and B). Since we are *inter alia* interested in the behavior of these profiles close to the critical temperature T_c, it is suitable to express the temperature dependence in terms of the reduced temperature $\tau=(T_c-T)/T_c$. The fact that for $T\to T_c$ the scaling properties of the surface tension and of the density profile are well known due to general arguments allows us to test successfully for the present model the reliability of our numerical results in this limit. This enables us to apply the same kind of analysis to the scaling behavior of the orientational order and of the anisotropic part of the surface tension which have not yet been studied before.

A. Dependence on the strength of the dipoles

While the critical density ρ_c depends only weakly on m [4], $T_c(m)$ increases significantly for larger values of m; in Fig. 1 this dependence on m is expressed in terms of the dimensionless dipole strength $m^*=[m^2/(\sigma^3\varepsilon)]^{1/2}$ and the dimensionless temperature $T^*=k_BT/\varepsilon$. For small m we corroborate the prediction by Yang *et al.* [9]:

$$T_c(m\to0)-T_c(m=0)\sim m^4\ . \tag{3.1}$$

In Fig. 2 we show the dependence of the dimensionless number density profile $\rho^*(z)=\rho(z)\sigma^3$ on the strength of the dipoles at a fixed reduced temperature. Its position $z=0$ is defined by $\rho(z=0)=(\rho_l+\rho_g)/2$. A higher resolution reveals that these curves do not intersect at a single common point. [$\rho(z)$ corresponds to a particular mean-field approximation for the so-called intrinsic liquid-vapor interface [7].] The main dependence of $\rho(z)$ on m is due to the increase of ρ_l and the decrease of ρ_g, respectively, for larger m. Correspondingly the number density profile sharpens as function of m. For a subset of m values Fig. 3 shows the corresponding orientational order

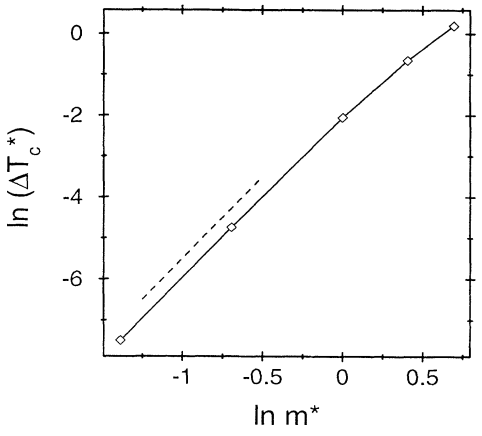

FIG. 1. Shift of the bulk critical temperature $\Delta T_c^* = T_c^*(m^*) - T_c^*(0)$ as a function of the strength m^* of the dipoles (full curve). The dashed line indicates the slope expected from Eq. (3.1).

profiles $\alpha_2(z)$. The position $z=0$ is fixed by the corresponding one for $\rho(z)$ (see above). The numerical data reveal that in general $\alpha_2(z=0)$ is nonzero. Both the width of the profile $\alpha_2(z)$ and the zero of $\alpha_2(z)$ depend only weakly on m. In contrast, however, the orientational order increases significantly for larger m. Both the minimum and maximum values of $\alpha_2(z)$ vary $\sim m^4$ for $m \to 0$ (see the inset of Fig. 3). It is interesting that $\langle \alpha_2 \rangle = \int_{-\infty}^{\infty} dz\, \alpha_2(z)$ is nonzero and follows the same power law as a function of m for any fixed reduced temperature. Since the bulk phases are isotropic $\alpha_2(z)$ vanishes for $|z| \to \infty$. The above power laws lead to a dimensionless limiting function

$$\mathcal{A}_2(z/\sigma) = \lim_{m \to 0} [\alpha_2(z/\sigma)/m^{*4}] . \tag{3.2}$$

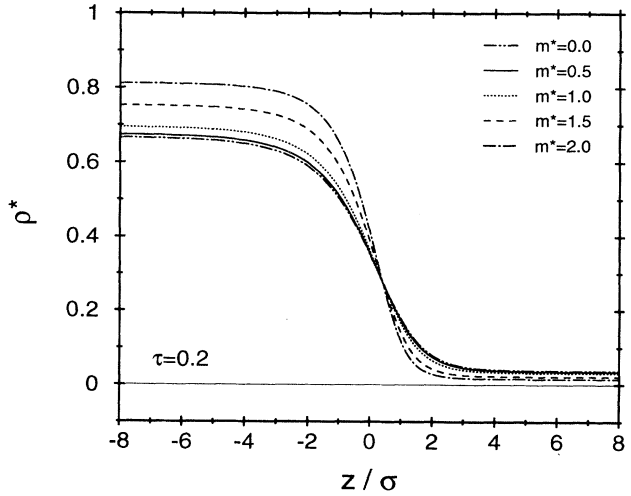

FIG. 2. Dependence of the number density profile on the strength of the dipoles at a fixed reduced temperature $\tau=0.2$.

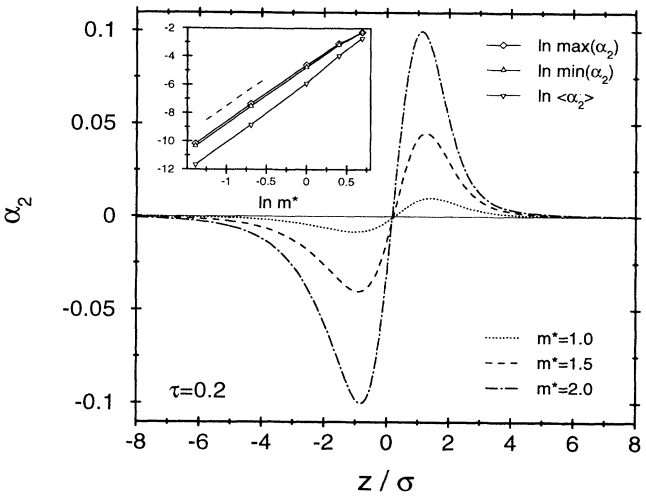

FIG. 3. Dependence of the orientational order profile $\alpha_2(z)$ on the strength of the dipoles. The values of m and τ are such that Fig. 2 displays the corresponding number density profiles; $\alpha_2(z) \equiv 0$ for $m=0$. On the given scale $\alpha_2(z)$ is invisible for $m^*=0.5$. The inset shows that the maximum, the minimum, and $\langle \alpha_2 \rangle = \int_{-\infty}^{\infty} dz\, \alpha_2(z)$ vanish $\sim m^4$ (dashed line) for $m \to 0$. Here and in Fig. 2 the various symbols for the lines have been assigned such that one type of line describes the same system.

Figure 4 shows how $\mathcal{A}_2(z/\sigma)$ is reached for $m \to 0$ at a fixed reduced temperature τ.

B. Temperature dependence and scaling properties

In Sec. III A we varied the strength of the dipole moments at a fixed reduced temperature τ. In this section we analyze systematically the temperature dependence of both the number density and orientational order profiles for a fixed value ($m^*=1.5$) of the dipole strength. Figure 5 displays the broadening of the number density

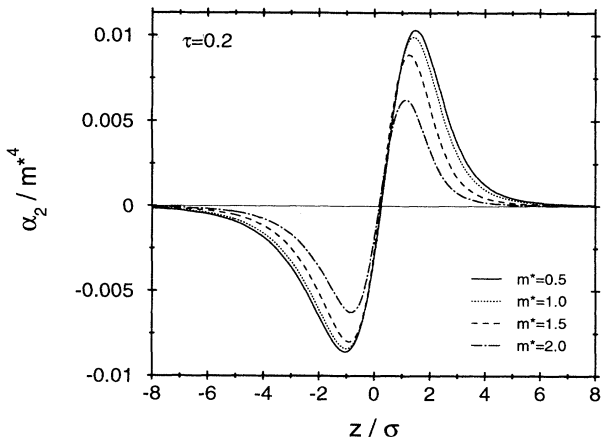

FIG. 4. At any fixed temperature $\alpha_2(z)/m^{*4}$ reduces to a limiting function for $m \to 0$ [see Eq. (3.2)]. The full line is a close approximation of this function $\mathcal{A}_2(z)$.

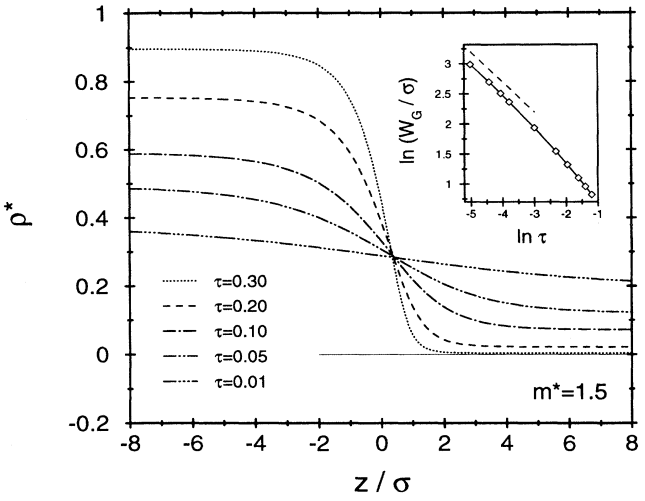

FIG. 5. Dependence of the number density profile on temperature τ for a fixed value $m^*=1.5$. The inset displays the divergence of the width of the interface $W_G(\tau\to 0)\sim\tau^{-\nu}$ [see Eqs. (3.3) and (3.4)] for $\tau\to 0$. The dashed line in the inset indicates the mean-field power law $\nu=\frac{1}{2}$.

profiles upon approaching criticality, i.e., $\tau\to 0$. As before the position $z=0$ is defined by $\rho(z=0)=(\rho_l+\rho_g)/2$ and the profiles actually do not intersect at a single common point. Following Ref. [10] we define the width of the interface as

$$W_G=-(\rho_l-\rho_g)\left[\frac{d\rho(z)}{dz}\right]^{-1}\Bigg|_{z=z_G}, \tag{3.3}$$

where z_G is the position of the Gibbs dividing surface:

$$\int_{-\infty}^{z_G} dz'[\rho_l-\rho(z')]=\int_{z_G}^{\infty} dz'[\rho(z')-\rho_g]\ . \tag{3.4}$$

Close to T_c, W_G diverges as

$$W_G(\tau\to 0)\sim\tau^{-\nu}\ , \tag{3.5}$$

where ν is the critical exponent of the diverging bulk correlation length $\xi(\tau\to 0)\sim\tau^{-\nu}$. The inset of Fig. 5 supports this result with $\nu=\frac{1}{2}$ for the mean-field theory used here. Close to criticality the number density profiles are expected to exhibit a scaling form governed by a universal scaling function $F_\rho(y)$,

$$\rho(z,\tau\to 0)=\rho_c+A_\rho\tau^\beta F_\rho(z/\xi)\ , \tag{3.6}$$

where ρ_c is the critical density and A_ρ the nonuniversal amplitude of the bulk order parameter:

$$\rho_l(\tau\to 0)-\rho_c=A_\rho\tau^\beta=\rho_c-\rho_g(\tau\to 0)\ . \tag{3.7}$$

Within mean-field theory $\beta=\frac{1}{2}$ and $F_\rho(y)=-\tanh(y/2)$. Here we used the following definition for the correlation length ξ:

$$\xi^2=\frac{1}{6}\frac{\int d^3r\, r^2 G(r)}{\int d^3r\, G(r)} \tag{3.8}$$

based on the two-point correlation function in the bulk

$$G(r=|\mathbf{r}_1-\mathbf{r}_2|)=\langle\rho(\mathbf{r}_1)\rho(\mathbf{r}_2)\rangle-\langle\rho(\mathbf{r}_1)\rangle\langle\rho(\mathbf{r}_2)\rangle\ . \tag{3.9}$$

Within our model one has

$$\xi=\left[\frac{|g_2|}{6\left[\dfrac{\partial^2 f_{\rm ref}^{\rm HS}}{\partial\rho^2}+g_0\right]}\right]^{1/2}, \tag{3.10}$$

where

$$g_n=\frac{4\pi}{\beta}\int_\sigma^\infty dr\, r^{n+2}\left\{1-e^{-\beta\omega_{\rm LJ}(r)}\times\int_0^1 dx\, i_0(Z(1+3x^2)^{1/2})\right\}; \tag{3.11}$$

here $Z=\beta m^2/r^3$ and $i_0(y)$ is defined in Eq. (A9) of Appendix A. Below T_c Eq. (3.10) leads to two different correlation lengths ξ_l and ξ_g in the liquid and vapor phase, respectively, which become identical in the limit $\tau\to 0$. Figure 6 shows how the density profiles reduce to the above scaling form for $\tau\to 0$.

Since $\rho-\rho_c$ is the order parameter, the scaling form in Eq. (3.6) is expected on general grounds. On the other hand, *a priori* it is unclear whether the orientational order profile $\alpha_2(z,\tau\to 0)$ also takes on a scaling form. In Fig. 7 we show the broadening and the reduction of the orientational order at the interface upon increasing the temperature for a fixed value $m^*=1.5$. A natural measure for the width W_{α_2} of the orientational profile $\alpha_2(z)$ is given by the distance $z_{\max}-z_{\min}$ between the positions of the extrema of $\alpha_2(z)$: $\max(\alpha_2)=\alpha_2(z=z_{\max}>0)>0$ and $\min(\alpha_2)=\alpha_2(z=z_{\min}<0)<0$. According to the upper

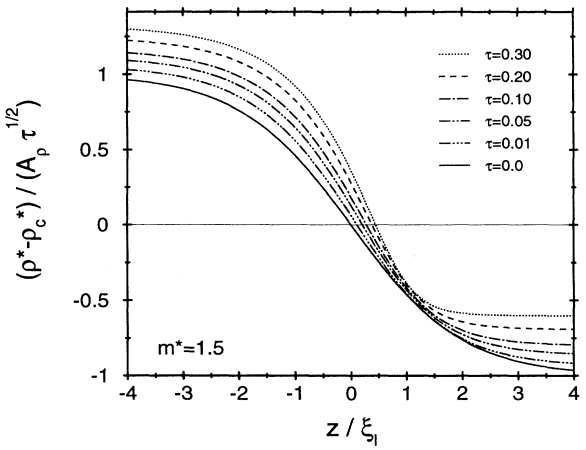

FIG. 6. Number density profiles in scaling form for $m^*=1.5$. ξ_l is the correlation length in the liquid phase [see Eqs. (3.8)–(3.11)]. A_ρ is the nonuniversal amplitude of the bulk order parameter [Eq. (3.7)]. In the limit $\tau\to 0$ the scaled profiles reduce to the universal scaling function $F_\rho(y)=-\tanh(y/2)$ [Eq. (3.6)].

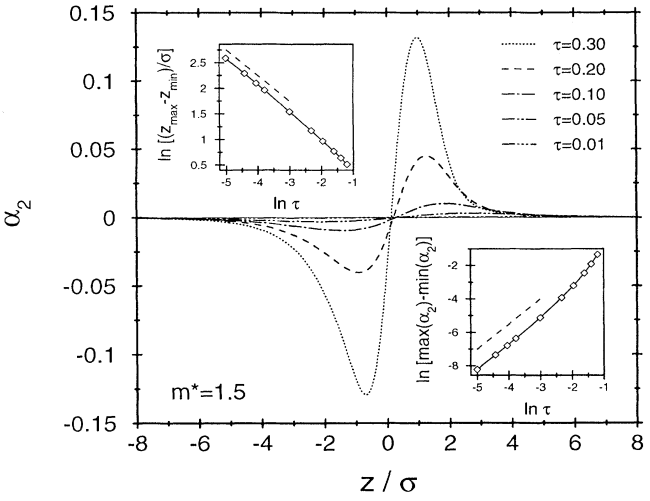

FIG. 7. Broadening and reduction of the orientational order $\alpha_2(z)$ upon increasing the temperature $\tau \to 0$ for $m^* = 1.5$. The upper left inset shows that the width of this profile $W_{\alpha_2} = z_{\max} - z_{\min}$ diverges as $\tau^{-1/2}$ for $\tau \to 0$ (the dashed line indicates the slope $-\frac{1}{2}$). The lower right inset demonstrates that the strength of the orientational order $D_{\alpha_2} = \max(\alpha_2) - \min(\alpha_2)$ vanishes as $\tau^{3/2}$ for $\tau \to 0$ (the dashed line indicates the slope $\frac{3}{2}$).

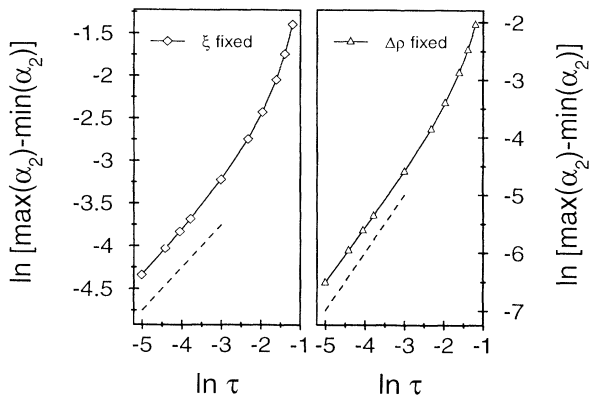

FIG. 8. Decrease of the orientational order $D_{\alpha_2} = \max(\alpha_2) - \min(\alpha_2)$ in the limit $\tau \to 0$ if ξ is kept fixed artificially and $\Delta\rho \sim \tau^{1/2}$ (left part) or if $\Delta\rho$ is kept fixed artificially and ξ diverges $\sim \tau^{1/2}$ (right part). In the first case one finds $D_{\alpha_2}(\tau \to 0) \sim \tau^{1/2}$ whereas in the second case $D_{\alpha_2}(\tau \to 0) \sim \tau$. The dashed lines indicate the slopes $\frac{1}{2}$ and 1, respectively. Note the difference in scale between the left and right part of the figure.

left inset of Fig. 7 we find that W_{α_2} is proportional to the bulk correlation length:

$$W_{\alpha_2} = z_{\max} - z_{\min} \sim \tau^{-\nu}, \quad \tau \to 0, \tag{3.12}$$

with $\nu = \frac{1}{2}$ within mean-field theory.

The degree of the orientational order at the interface can be measured by the difference (see the lower right inset of Fig. 7)

$$D_{\alpha_2} = \max(\alpha_2) - \min(\alpha_2) \sim \tau^{3/2}, \quad \tau \to 0. \tag{3.13}$$

In order to interpret this power law beyond mean-field theory we minimized the grand-canonical variational functional in that subspace of profiles for which the thickness W_G of the density profiles and thus the bulk correlation length ξ are kept fixed artificially but for which the density difference $\Delta\rho$ vanishes as $\tau^{1/2}$. In this case we find $D_{\alpha_2}(\tau \to 0) \sim \tau^{1/2}$ (see the left part of Fig. 8). On the other hand, if $\Delta\rho$ is kept fixed artificially, but ξ diverges as $\tau^{-1/2}$, we find $D_{\alpha_2}(\tau \to 0) \sim \tau \sim \xi^{-2}$ (see the right part of Fig. 8). This leads us to the conjecture

$$D_{\alpha_2}(\tau \to 0) \sim \tau^{\beta + 2\nu}. \tag{3.14}$$

Equations (3.12) and (3.14) can be combined to the following scaling form for $\alpha_2(z,\tau)$:

$$\alpha_2(z, \tau \to 0) = \tau^{\beta + 2\nu} \bar{F}_{\alpha_2}(z/\xi). \tag{3.15}$$

Figure 9 shows that for m^* fixed indeed $\lim_{\tau \to 0}[\tau^{-3/2} \alpha_2(z/\xi, \tau)]$ reduces to a limiting function $\bar{F}_{\alpha_2}(y)$. Future investigations should reveal whether, apart from a nonuniversal amplitude B, the scaling function $F_{\alpha_2}(y)$ can be expressed in terms of a universal function $F_{\alpha_2}(y) = \bar{F}_{\alpha_2}(y)/B$ which is independent of, e.g., the potential parameters m, ε, and σ as well as of the form of the interaction potentials. [The function $F_\rho(y)$ is known to be universal in that sense.]

The common characteristic feature of all orientational order profiles $\alpha_2(z)$ is that they are negative on the liquid side and positive on the vapor side. This means that in the region with the higher number density the dipoles are preferentially orientated parallel to the plane of the mean

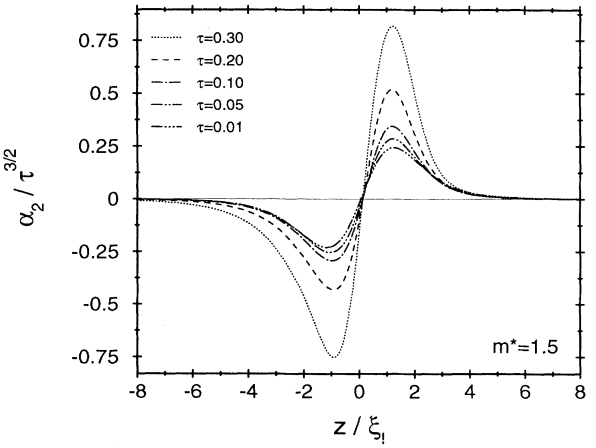

FIG. 9. In the limit $\tau \to 0$ and m^* fixed the orientational profile reduces to a scaling form $\alpha_2(z, \tau \to 0) = \tau^{3/2} \bar{F}_{\alpha_2}(z/\xi)$ [see Eq. (3.15)]. Here z is measured in units of the correlation lengths ξ_l of the bulk liquid phase. The symbols of the various curves correspond to those used in Figs. 5–7.

interface whereas in the region with the lower number density the dipoles are preferentially orientated orthogonal to it. (Of course there is no net polarization on either side, i.e., $\alpha_1 \equiv 0$ [compare Eq. (4.24) in Ref. [4]]). Qualitatively this preference can be understood by considering two homogeneous half-spaces $z>0$ and $z<0$ which are filled by dielectrics with permittivity ϵ_+ and ϵ_-, respectively [11]. The energy E required to place a dipole $\mathbf{m}$ with a fixed angle θ between the z axis and $\mathbf{m}$ at a distance $z>0$ from the sharp interface at $z=0$ is given by

$$E=-\frac{m^2}{16}\frac{\epsilon_- -\epsilon_+}{\epsilon_+(\epsilon_- +\epsilon_+)}\frac{1+\cos^2\theta}{z^3} . \tag{3.16}$$

At a fixed distance z, E attains its minimum value for $\theta=0$ and π if $\epsilon_+<\epsilon_-$ and for $\theta=\pi/2$ if $\epsilon_+>\epsilon_-$. Thus the preferred orientation of the dipole is either parallel or antiparallel to the normal of the interface if it is located in the medium with the smaller permittivity and parallel to the interface if the dipole is located in the medium with the larger permittivity. Since the permittivity increases as a function of the number density this observation is in accordance with the signs of $\alpha_2(z)$ on both sides of the interface.

IV. SURFACE TENSION

The knowledge of the profiles of the number density and of the orientational order enables one to compute the surface tension $\gamma_{l,g}$ of the liquid-vapor interface of Stockmayer fluids. According to Eqs. (4.34)–(4.37) in Ref. [4] one obtains three distinct contributions,

$$\gamma_{l,g}=\gamma_{l,g}^{(\rho)}+\gamma_{l,g}^{(\mathcal{S})}+\sum_{\Lambda\,[\neq(000)]}\gamma_{l,g}^{(\Lambda)} , \tag{4.1}$$

which are given by the density profile alone, by a purely entropic contribution $\mathcal{S}$, and by the deviation from isotropy, where $\Lambda=(l_1 l_2 l)\in\mathbb{N}^3$, respectively. In the following $\gamma_{l,g}^{*}=\gamma_{l,g}\sigma^2/\varepsilon$ denotes the dimensionless total surface tension and

$${}^{a}\gamma_{l,g}^{*}=\gamma_{l,g}^{*}-\gamma_{l,g}^{(\rho)}\sigma^2/\varepsilon \tag{4.2}$$

the so-called anisotropic contribution to the total surface tension. We want to emphasize that ${}^{a}\gamma_{l,g}^{*}$ is only due to the missing isotropy at the interface so that $\gamma_{l,g}^{(\rho)}\sigma^2/\varepsilon$ also depends on the strength of the dipoles: $\gamma_{l,g}^{(\rho)}\neq 0$ even for $\varepsilon=0$, i.e., for a fluid with purely dipolar interactions. The explicit expressions for these three contributions are given in Appendix C.

A. Total surface tension

Based on the profiles of the number density and of the orientational order the formulas in Appendix C lead to the temperature and m dependence of the total surface tension as shown in Fig. 10. For small dipole moments the surface tension increases only slightly as a function of m whereas for $m^*>1$ this increase is much stronger. For $m^*\geq 0.5$, $\gamma_{l,g}$ is roughly proportional to m^3. The surface tension increases for temperatures further apart from $T_c(m)$ stronger as a function of m than closer to T_c.

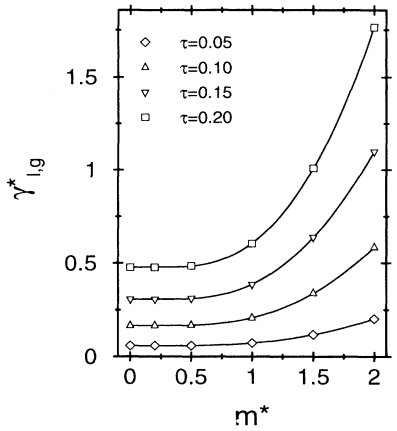

FIG. 10. Dimensionless total surface tension $\gamma_{l,g}^{*}=\gamma_{l,g}\sigma^2/\varepsilon$ as a function of the dimensionless strength of the dipoles $m^*=m\sigma^{-3/2}\varepsilon^{-1/2}$ for various reduced temperatures $\tau=(T_c-T)/T_c$. Note that T_c increases as function of m (see Fig. 1).

[Note that an increase of m and $\tau=$const correspond to an increase in temperature $T=(1-\tau)T_c(m)$ because $T_c(m)$ increases as function of m (see Fig. 1).] In Fig. 11 we show the dependence on τ of the ratio of $\gamma_{l,g}(m)$ and its value $\gamma_{l,g}(m=0)$ for the corresponding pure Lennard-Jones system. We find that this ratio deviates significantly from 1, but varies only slightly as function of τ. This means that the dipolar interaction can increase the absolute value of the surface tension substantially, but the temperature dependence is still mainly governed by the equivalent Lennard-Jones system, i.e., one with the same critical temperature as the Stockmayer fluid. Note that the ratio shown in Fig. 11 compares either the surface tensions of two systems with the same Lennard-Jones contribution to the interaction but at different tem-

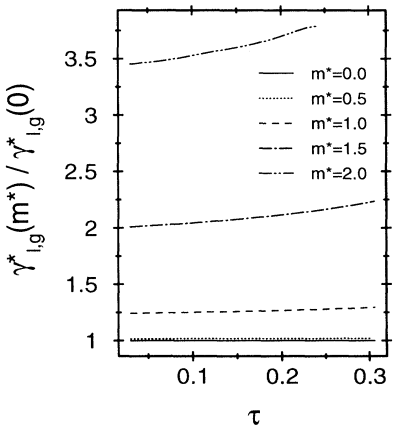

FIG. 11. The ratio of $\gamma^*[m^*, T=(1-\tau)T_c(m^*)]$ and $\gamma^*[m^*=0, T=(1-\tau)T_c(0)]$ as a function of τ for various values of m^*. Although this ratio differs significantly from 1, it varies only slightly as a function of τ.

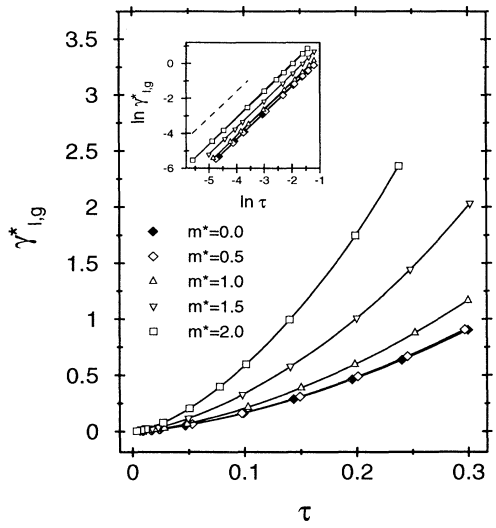

FIG. 12. Temperature dependence of the total surface tension for various strengths of the dipoles. According to the inset $\gamma_{l,g}$ vanishes $\sim\tau^{3/2}$ for $\tau\to 0$ (dashed line).

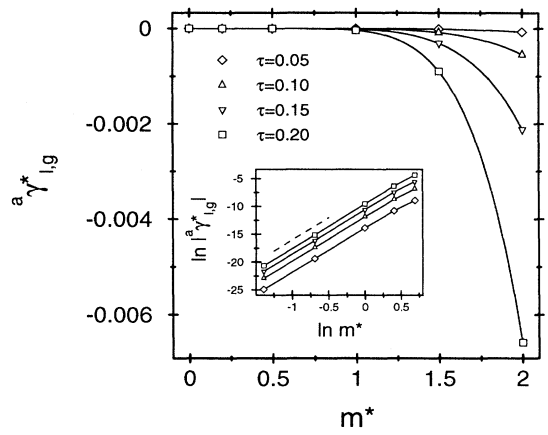

FIG. 13. Dependence of the dimensionless anisotropic contribution to the surface tension on the dimensionless strength of the dipole moments for four different reduced temperatures. The inset shows that $^a\gamma_{l,g}(m\to 0,\tau)\sim m^8$ (dashed line). One should compare Fig. 10.

peratures, $\gamma^*[m^*,T=(1-\tau)T_c(m^*)]/\gamma^*[m^*=0,T=(1-\tau)T_c(0)]$, or two systems at the same temperature T but with different Lennard-Jones contributions such that $T_c(m,\varepsilon_1)=T_c(0,\varepsilon_2)$. In Ref. [4] we showed that the *bulk* properties of a Stockmayer fluid follow (within our model exactly) from an effective temperature-dependent and isotropic potential (see Sec. III A in Ref. [4]), which at large distances behaves like a Lennard-Jones potential. Figure 11 suggests that approximately the temperature dependence of the *surface tension* of a Stockmayer fluid is that of an equivalent pure Lennard-Jones system.

In d spatial dimensions the surface tension vanishes as $\tau^{(d-1)\nu}$ for $\tau\to 0$. Mean-field theory corresponds to $d=4$ and $\nu=\frac{1}{2}$ so that $\gamma^{\mathrm{MFT}}_{l,g}(\tau\to 0)=\gamma_0\tau^{3/2}(1+\cdots)$. Figure 12 is in accordance with this power law. The inset of Fig. 12 shows that the correction terms to the leading behavior are very small even far away from $T_c(m)$. The amplitude γ_0 increases as function of m.

B. Anisotropic contribution to the surface tension

According to Eq. (4.2) and Appendix C the anisotropic contribution $^a\gamma_{l,g}$ to the total surface tension describes all those terms of the total surface tension which vanish if the explicit dependence on $\alpha_2(z)$ is neglected. (Note that this is not equivalent to the limit $m\to 0$.) Figure 13 displays the dependence of $^a\gamma^*_{l,g}=\,^a\gamma_{l,g}\sigma^2/\varepsilon$ on the strength of the dipoles for four reduced temperatures. We find that $^a\gamma_{l,g}$ is negative. However, its absolute value is drastically smaller than the total surface tension: $|^a\gamma_{l,g}|/\gamma_{l,g}\simeq\frac{1}{300}$, $\frac{1}{500}$, and $\frac{1}{1000}$ for $\tau=0.2$, 0.15, and 0.1, respectively (see Fig. 10). This means that the main influence of an additional dipolar interaction potential on the surface tension is due to the change of the bulk phase diagram, of the number densities of the coexisting phases, and of their profile through the interface, but not due to preferential orientations at the interface. The absolute value of the anisotropic contribution to the surface tension is largest at low temperatures. As shown by the inset in Fig. 13 we find

$$^a\gamma_{l,g}(m\to 0,\tau)\sim m^8\ . \tag{4.3}$$

The comparison with Fig. 10 shows that $^a\gamma_{l,g}(m)$ vanishes much more rapidly for $m\to 0$ than $\gamma_{l,g}(m)-\gamma(0)$. The same is true for the dependence of $^a\gamma_{l,g}$ on the reduced temperature τ, which is shown in Fig. 14 for vari-

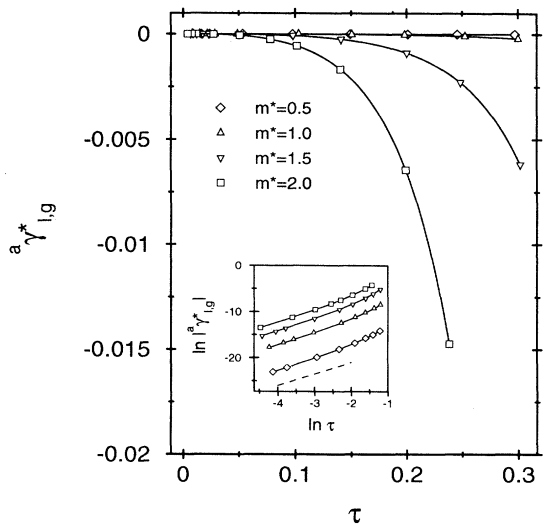

FIG. 14. Dependence of the dimensionless anisotropic contribution to the surface tension on the reduced temperature τ for four different strengths of the dipole moments. As indicated by the dashed straight line in the inset one finds $^a\gamma_{l,g}(\tau\to 0)\sim\tau^{5/2}$. One should compare these data with those in Fig. 12.

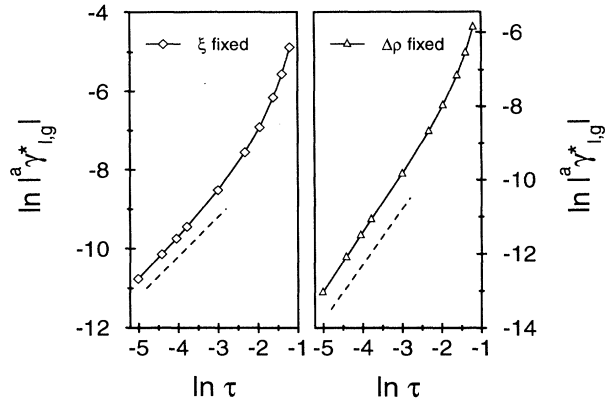

FIG. 15. Vanishing of the anisotropic contribution to the surface tension in the limit $\tau \to 0$ if ξ is kept fixed artificially and $\Delta\rho \sim \tau^{1/2}$ (left part) or if $\Delta\rho$ is kept fixed artificially and ξ diverges $\sim \tau^{-1/2}$ (right part). In the first case one finds ${}^a\gamma_{l,g}(\tau \to 0) \sim \tau$ whereas in the second case ${}^a\gamma_{l,g}(\tau \to 0) \sim \tau^{3/2}$. The dashed lines indicate the slopes 1 and $\frac{3}{2}$, respectively.

ous dipole moments. We find ${}^a\gamma_{l,g}(\tau \to 0) \sim \tau^{5/2}$ compared with $\gamma_{l,g}(\tau \to 0) \sim \tau^{3/2}$ (see Fig. 12). These power laws ensure that $\gamma_{l,g}$ remains positive although ${}^a\gamma_{l,g}$ is negative. One should note that the temperature dependence of ${}^a\gamma_{l,g}$ is enhanced significantly by strong dipole moments.

In order to interpret this power law of ${}^a\gamma_{l,g}(\tau \to 0)$ we have proceeded as in Sec. III B, leading to Eq. (3.14). There we have produced profiles of both the number density and the orientational order either for $\Delta\rho(\tau \to 0) \sim \tau^{1/2}$ under the constraint $\xi = \text{const}$ or for $\xi(\tau \to 0) \sim \tau^{-1/2}$ under the constraint $\Delta\rho = \text{const}$. In the first case the corresponding anisotropic contribution to the surface tension vanishes proportional to τ whereas in the second case it vanishes $\sim \tau^{3/2}$ (see Fig. 15). This leads us to the conjecture

$$ {}^a\gamma_{l,g}(\tau \to 0) \sim \tau^{2\beta + (d-1)\nu} \tag{4.4}$$

compared with $\gamma_{l,g}(\tau \to 0) \sim \tau^{(d-1)\nu}$.

V. DISCUSSION

In this section we discuss our results by comparing them with those obtained in the literature previously. As already emphasized in the Introduction the status of the bulk properties of Stockmayer fluids has been analyzed in detail in Ref. [4]. Therefore in the following we focus on the structural and thermal properties of their liquid-vapor interface.

Due to the complexity of this problem there are only few numerical results available [12]. They indicate that the interfacial properties of molecular liquids depend sensitively on both the details of the intermolecular interaction potential and on the various applied approximation schemes for solving the corresponding statistical mechanics problem. Since in previous studies different approximation schemes have been applied for different interaction potentials, a coherent picture has hardly emerged with which we could compare our results. Therefore our comparisons with the literature are mostly limited to be qualitative ones. Since the virtues and drawbacks of previous analytical and numerical methods as compared to our approach have been discussed in detail in Sec. II A and Sec. VI of Ref. [4], we confine the following discussion to explicit numerical results.

A. Density and orientational profiles

By applying the so-called "f expansion" (see Sec. II A in Ref. [4]) to the Stockmayer model Gubbins and Thompson [13] have computed $\hat{\rho}_l(z) = \alpha_l(z)\rho(z)$ for $l = 0$, 2, 4, 6, 8 at a fixed temperature $T^* = 1.3$ and for $m^* = 1$, 1.5, and 2.0. (The authors doubt that their technique is reliable for $m^* \geq 2$.) For $m^* = 1.5$ their resulting orientational profile $\alpha_2(z)$ agrees qualitatively with ours presented in Figs. 3 and 7. Surprisingly, however, Gubbins and Thompson find that for the *smaller* value $m^* = 1.0$ the functions $\hat{\rho}_2(z)$ and, due to $\rho(z) > 0$, therefore also $\alpha_2(z)$ exhibit three zeros: one at $z \simeq 0$ and two on the liquid side of the interface at $z/\sigma \simeq -1.5$ and -2.1, respectively, so that $\alpha_2(z)$ turns positive between the latter ones (see Fig. 4 in Ref. [13]). This is in qualitative disagreement with our findings according to which for all m and τ, $\alpha_2(z)$ turns negative below $z \simeq 0$ and approaches 0 monotonically from below for $z \to -\infty$ after passing its minimum on the liquid side. [We would like to add that in many publications a precise definition of the position $z = 0$ is missing. Throughout the present paper $z = 0$ is defined by $\rho(z = 0) = (\rho_l + \rho_g)/2$ (see Sec. III A).] On the other hand, results obtained by a different perturbation expansion in the frame-work of the density-functional theory [14] are again in qualitative agreement with our present result. However, these authors consider systems governed by the sum of dispersion, overlap, quadrupole-quadrupole, dipole-dipole, dipole-quadrupole, and isotropic forces. Since their first-order perturbation theory does not predict any orientational order at the interface for, e.g., pure dipole-dipole interactions, their results cannot be compared with ours. Furthermore, these authors confine their analysis to a small subspace of allowed distribution functions (see also below).

Eggebrecht, Gubbins and Thompson [15] have extended the f expansion technique for a Stockmayer fluid mentioned above [13] to a wider range of temperatures and dipole moments and in addition they applied an Yvon-Born-Green (YBG) type of integral equation for describing the liquid-vapor interface. Their f expansion yields lower values for T_c, $(m^*, T_c^*) = (0, 1.26), (0.5, 1.29), (1, 1.41), (1.5, 1.73), (2, 2.26)$, as compared to our approach [4] which leads to $(m^*, T_c^*) = (0, 1.343), (0.5, 1.352), (1, 1.472), (1.5, 1.862), (2, 2.560)$. In order to enable a reasonable quantitative comparison in the following we consider always reduced temperatures $\tau = 1 - T/T_c$. The overall features of the number density profiles are similar to those shown in Figs. 2 and 5. However, there are important differences. First, Eggebrecht, Gubbins, and Thompson [15] consider only density

profiles of the form of the hyperbolic tangent, i.e., $\rho(z)=(\rho_l e^{-\alpha z}+\rho_g)(e^{-\alpha z}+1)^{-1}$, where α is the only remaining free variational parameter. Figure 6 shows that away from T_c this represents only a poor approximation to the actual shape of the profile. *Inter alia* the hyperbolic tangent ansatz misses the van der Waals tails of the density profile (see, e.g., Ref. [7]). Furthermore, this ansatz means that the *shape* of the profile is the same for all temperatures and dipole moments. If one takes the numerical data in Fig. 9 of Ref. [15] for their width $D\equiv 4/\alpha$ and evaluates them at a fixed reduced temperature $\tau=0.2478$ one obtains the following results for the four dipole strengths considered: $(m^*,D/\sigma)=(0,2.55),(1,2.3),(1.5,\ 2.3),(2,3.0)$. Thus their results imply that, for τ fixed, an increase of the dipole strength first leads to a sharpening of the density profiles, to a minimum value of the thickness at $m^*\simeq 1.25$, and finally to a broadening for even larger values of m^*. This behavior must be contrasted with our results in Fig. 2 from which one can infer that for a fixed value of τ the density profiles monotonically sharpen upon an increase of the dipole strengths. According to Figs. 12–14 in Ref. [15] the orientational profiles $\alpha_2(z)$ for $(m^*,T^*)=(1,0.75)$, (1.5,1.0), and (2,1.5) as obtained by the f-expansion technique are in qualitative agreement with those shown in our Figs. 3 and 7. *A fortiori* it is surprising that according to Refs. [13] and [15] within the same technique only the system with $m^*=1.0$ at the temperature $T^*=1.3$ exhibits a qualitatively different behavior (see above and Fig. 4 in Ref. [13]). The predictions for $\alpha_2(z)$ of the angular YBG equation [15] are at variance both with those of the f expansion and ours. They yield always a positive maximum of $\alpha_2(z)$ on the liquid side at $z/\sigma\simeq -1.5$ and either two or even three zeros. For $(m^*,T^*)=(1.0,0.75)$ and (2.0,1.5), $\alpha_2(z\to-\infty)$ approaches zero from above in contrast to our findings $\alpha_2(z\lesssim 0)<0$.

In a second paper the same authors have published molecular-dynamics data for the liquid-vapor interface of Stockmayer fluids [16]. These simulations provided the profiles $\rho(z)$ and $\hat{\rho}_2(z)$ for $(m^*,T^*)=(1,1.01)$ and (2,1.52). Since in this work T_c^* has not been determined, the above two values of T^* cannot be expressed reliably in terms of τ. Whereas the number density profiles $\rho(z)$ are smooth and in qualitative agreement with our results, the function $\hat{\rho}_2(z)$ for $(m^*,T^*)=(2,1.52)$ [for the other system $\hat{\rho}_2(z)$ was not detectable due to the smallness of the effect [16]] exhibits many rapid changes within the investigated interval $-4\sigma\le z\le 3\sigma$. Since for these data no error bars are given, it is unclear to which extent these rapid changes are due to numerical noise or due to real intrinsic structures of the profile. The main feature of the simulated data for $\hat{\rho}_2(z)$ is that it is negative for $|z/\sigma|\lesssim 2$. For $z\le -2\sigma$, $\hat{\rho}_2(z)$ seems to oscillate around zero with a preference for negative values whereas for $z\ge 2\sigma$ it is practically zero. The expected positive maximum on the vapor side does not show up. In view of the long range of the intermolecular potential and the smallness of $\alpha_2(z)$ further simulation data with an increased size of the simulation cell (Ref. [16], $20\times 18^2\sigma^3$) and with a large number of particles (Ref. [16], 144) would be highly welcome.

More recently Teixeira and Telo da Gama [17] employed a density-functional theory for Stockmayer fluids which they compared with the simulation results in Ref. [16]. Their approach is similar to ours but differs in two respects: (i) In Eq. (2.6) Teixeira and Telo da Gama expand the exponential $e^{-\beta w_{ex}}$ and they keep only the term quadratic in w_{ex} (the term linear in w_{ex} gives 0). (ii) For the isotropic part of the interaction potential Teixeira and Telo da Gama do not use a Lennard-Jones potential [Eq. (2.3)] but a potential which is infinitely repulsive for $r\le\sigma$ and equals $-4\varepsilon(\sigma/r)^6$ for $r>\sigma$. Note that the depth of this potential is 4ε instead of ε as for a full Lennard-Jones potential. Nevertheless Teixeira and Telo da Gama use $m^*=(m^2/\sigma^3\varepsilon)^{1/2}$ as the reduced strength of the dipole moment and the reliability of their truncated expansion depends on the value of *this* quantity. While (ii) represents only a quantitative but no conceptual difference to our approach, (i) amounts to a much more relevant difference. The aforementioned expansion of the exponential is equivalent to a perturbation theory in powers of the dipole strength truncated after the lowest nontrivial term. This truncation limits the applicability of that approach to small values of m^*. In a later extension of their work to experimentally relevant binary liquid mixtures [18] (CH_3I+CCl_4 and $CH_3CN+CCl_4$) the authors realized that the experimental value $m=4.7$ D (1D = 1 Debye $=10^{-18}$ erg$^{1/2}$ cm$^{3/2}$) for CH_3CN is too large in order to be treated by their truncated expansion; together with $\sigma=4.499$ Å and—depending on their two choices as a model parameter (see Table IV in Ref. [18])—$\varepsilon=3.04\times10^{-14}$ or 5.92×10^{-14} erg this corresponds to $m^*=2.83$ or 2.02, respectively. (Instead the authors decided to model CH_3CN by $m=2.41$ D, $\sigma=4.499$ Å, and $\varepsilon=3.04\times10^{-14}$ erg leading to $m^*=1.45$, which is still rather large.) The situation is more favorable for the truncated expansion in the case of CH_3I, which corresponds to $m^*=0.69$ or 0.93 for $m=1.62$ D, $\sigma=4.499$ Å, and $\varepsilon=6.05\times10^{-14}$ or 3.32×10^{-14} erg, respectively (see Table IV in Ref. [18]). In order to pinpoint the relevance of the truncation approximation in Refs. [17] and [18] without having the additional disturbing influence of using different interaction potentials [see (ii) above] we have repeated our approach for the model potential used in Refs. [17] and [18]. We have found that the truncated version underestimates the value of T_c by 10% in the absence of dipolar interactions; this discrepancy increases to 18% for $m^*=2$. A detailed comparison between the two approaches is given in Appendix A of Ref. [4]. Putting aside these quantitative differences the profiles of the number density and of the orientational order as obtained in Ref. [17] agree qualitatively with those given in Figs. 2, 3, 5, and 7. In addition, our present study goes beyond those in Refs. [17] and [18] as far as the systematic analysis of the dependences of the profiles on m and τ are concerned which lead to power laws and scaling properties.

Yang *et al.* [9,19] used the same kind of perturbation theory for the density functional as Teixeira and Telo da

Gama in order to study carefully the water liquid-vapor interface. Their approach differs from Ref. [17] in that the contribution to the density functional, which is quadratic in the anisotropic interaction, contains one additional term. Therefore also the approach by Yang *et al.* contains no terms in the density functional which are of higher order in the dipole strength but quadratic. Hence one must assume that their conclusions are also only reliable for small values of $m^*/\sqrt{T^*}$ (see below). As far as the isotropic part of the interaction potential is concerned Yang *et al.* use the same potential as Teixeira and Telo da Gama (see above), which differs from the Lennard-Jones potential which we use. In their effort to describe water Yang *et al.* include not only the dipole-dipole interaction, but, in addition, dipole-quadrupole and quadrupole-quadrupole interactions. This inclusion reduces the symmetry of the Hamiltonian and allows the authors to address the question, which part of the H_2O molecule at the interface points preferentially towards, e.g., the vapor phase. For a Stockmayer potential both directions have the same statistical weight. The isotropic and dipole part of the interactions are modeled by $m=2.1733$ D [9] and $m=2.1773$ D [19], respectively, $\varepsilon=1.0777\times10^{14}$ erg, and $\sigma=2.95$ Å [9,19]. This corresponds to $m^*=4.14$. In view of our above discussion this is an extremely large value of the reduced dipole strength for which we would expect the higher-order terms to be important. [Along the liquid-vapor coexistence line the temperature varies between $T_t\simeq273$ K and $T_c\simeq605$ K, which corresponds to $T_t^*=3.50$ and $T_c^*=7.75$, respectively, so that $m^*/\sqrt{T^*}$ (see below) varies between 1.50 at T_c and 2.2 at the triple point T_t. In both cases $m^*/\sqrt{T^*}$ is larger than 1 so that higher-order terms are important (see Sec. V C).] Therefore the comparison with experiments in Ref. [19] should be regarded with caution. Again, qualitatively the profiles of the number density and of the orientational order agree with those presented in Figs. 2, 3, 5 and 7.

At the end of this subsection we would like to mention that both $\rho(z)$ and $\alpha_2(z)$ approach their bulk values $\sim|z|^{-3}$. Badiali and co-workers [20–23] were able to derive rigorous expressions for the prefactors of these tails in $\rho(z)$ which are expressed in terms of the dielectric constant of the bulk phases. Similar results have also been derived by Lebovka, Ovcharenko, and Mank [24]. We leave it to a future study to compare these predictions with our model calculations.

B. Surface tension

As an excess quantity the surface tension is experimentally more easily accessible than local quantities such as the profiles of the number density or the orientational order. Therefore the question how the molecular structure of the interacting particles influences the surface tension has attracted considerable interest for many years [12]. In particular one would like to know how the surface tension changes if the anisotropic dipole-dipole interaction is added to an isotropic Lennard-Jones potential. Within the Fowler approximation, i.e., by assuming $\rho(z)=\rho_l\Theta(-z)$ and $\alpha_2(z)=0$, Gray and Gubbins [25] and Haile, Gray, and Gubbins [26] found that at $T^*=1.273$, γ increases by about 110% for $m^*=1.5$. This is in fair agreement with our findings which in this case predict an increase between 100% and 125% depending on the temperature. [In Refs. [25] and [26] the value of T_c^* is not given so that a quantitative comparison of the absolute values for γ is difficult. For our model $T_c^*(m=0)=1.343$ (see Ref. [4]) so that $T^*=1.273$ would correspond to $\tau\simeq0.05$, which is very small for the Fowler approximation. In this case we get $\gamma^*(m^*=0)\simeq0.05$ compared with $\gamma^*\simeq0.45$ in the Fowler approximation of Refs. [25] and [26].]

Eggebrecht, Gubbins, and Thompson [15] have calculated the liquid-vapor surface tension of a Stockmayer fluid beyond the Fowler approximation. (In fact, these authors neglected what we call the anisotropic contribution to the surface tension; according to Sec. IV B the resulting error is indeed small.) If one translates the results of Fig. 15 in Ref. [15] in our language, one finds the following dependence of γ^* on m^*: for $\tau=0.3$ one has $(m^*,\gamma^*)=(1.0,0.65),(1.5,0.75),(2.0,0.62)$, and for $\tau=0.2$ one has $(m^*,\gamma^*)=(1.5,0.35)$, (2.0, 0.3). Thus Eggebrecht, Gubbins, and Thompson find that for a fixed value of the reduced temperature τ the surface tension does not vary monotonically as function of m^*; for $\tau=0.3$ γ^* reaches a maximum at around $m^*=1.5$ whereas it decreases for $\tau=0.2$ as function of m^*. This is a qualitative difference to the behavior we find in Fig. 10, which states that for any τ, γ^* is a monotonically increasing function of m^*. As far as the absolute values are concerned we obtain larger values for γ^*: $(\tau,m^*,\gamma^*)=(0.3,1.0,1.17)$, (0.3,1.5,2.0), (0.2,1.5,1.0), (0.2,2.0,1.72). In a molecular-dynamics simulation for a Stockmayer fluid Eggebrecht, Thompson, and Gubbins [16] found $\gamma^*(T^*=1.01,m^*=1.0)=0.551$ whereas our corresponding results is γ^* $(\tau=0.28,m^*=1)=1.05$. This difference calls for two remarks. First, Eggebrecht, Thompson, and Gubbins finds for this system as coexisting bulk densities $\rho_l^*=0.702$ and $\rho_g^*=0.0023$, which differ from the corresponding values $\rho_l^*=0.75$ and $\rho_g=0.1$ obtained by Monte Carlo methods for the same system by Smit *et al.* [27]. Second, as shown in Fig. 6 of Ref. [4] $T^*=1$ is such a low temperature that there our density-functional theory starts to deteriorate yielding a too high density of $\rho_l^*=0.88$. Thus both in the simulations and in the density-functional theory the bulk properties of this thermodynamic state suffer from significant uncertainties so that the corresponding surface tension γ^* of this state carries a large error bar.

The surface tensions calculated by Teixeira and Telo de Gama [17] are in qualitative agreement with our results. A quantitative comparison is, however, only of limited use since, as described above, Teixeira and Telo da Gama use a different pair potential as we do. Generally speaking one finds that our surface tensions are larger, e.g., $\gamma^*(T^*=2,m^*=1.5)=0.21$ according to Ref. [17] whereas in our case the corresponding value is $\gamma^*(\tau=0.1,m^*=1.5)=0.34$.

The above discussion shows that up to now absolute values for the surface tension of dipolar liquids suffer from considerable uncertainties. Experimental results are

also of limited value in gauging the accuracy of the various theoretical approaches: first, it is difficult to assign reliable potential parameters σ, ε, and m to a given system; second, higher multipole moments contribute also to γ; and third, many-body forces have to be taken into account. For that reason Fig. 16 compares various results for the surface tension of a Lennard-Jones liquid with those of argon and xenon. DFT 1 denotes a simplified version of our density-functional approach which differs from it only insofar that the pair distribution function $g^{(2)}$ equals 1 (see, e.g., Ref. [28]). DFT 2 is the density-functional theory used in this paper. Ebner, Saam, and Stroud *et al.* [29] used the pair distribution function obtained from the Percus-Yevick theory (DFT 3). PT denotes the perturbation theory of Toxvaerd [30]. SIM 1 and SIM 2 correspond to Monte Carlo simulations by Liu [31] and to Monte Carlo and molecular-dynamics calculations by Salomons and Mareschal [32], respectively. These theoretical results are compared with experimental results (EXPT) for argon [33] with $\varepsilon/k_B=119.8$ K and $\sigma=3.405$ Å as well as for xenon [34] with $\varepsilon/k_B=229$ K and $\sigma=4.055$ Å; in reduced units $\gamma^*_{l,g}=\gamma\sigma^2/\varepsilon$ as a function of T/T_c the experimental data are—in accordance with the principle of corresponding states—very close (see Fig. 3 in Ref. [31]). Since the theoretical results lead to different values for T_c we have plotted $\gamma^*_{l,g}$ as a function of $\tau=1-T/T_c$ in order to suppress these differences. Note that this way of plotting the surface tension has a drawback for theories which predict inaccurate critical temperatures as, e.g., density-functional theories may do. Reducing the data by T_c will propagate this error into the noncritical region where these theories may actually be more accurate. This can lead to a shift of these theoretical data compared with the corresponding experimental ones. Nonetheless we adopt this kind of plot because it yields a convenient common temperature scale for different theoretical and experimental data. Although we did not try to collect all available theoretical and experimental data, Fig. 16 already tells that the absolute values for $\gamma^*_{l,g}$ differ significantly for various methods and with respect to the experimental data. These differences are larger for low temperatures. The density-functional theory used in this paper (DFT 2) has a tendency to overestimate the surface tension; this is in accordance with our previous observations for $m^*\neq 0$ (see above). The performance of the crude density-functional approach DFT 1 is surprisingly good. Nonetheless, one should keep in mind that *all* displayed results from analytic theories predict a wrong power law $\gamma_{l,g}(\tau\to 0)\sim\tau^{1.5}$ instead of $\tau^{1.26}$. We conclude by stating that the confidence level for the values of the surface tension of Stockmayer fluids is at most as "good" as that for the case $m=0$ shown in Fig. 16.

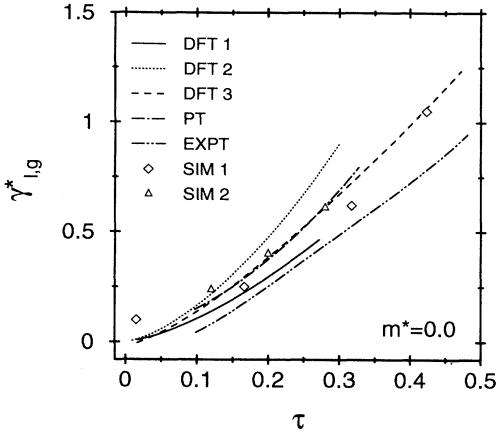

FIG. 16. Comparison of the reduced surface tension $\gamma^*_{l,g}=\gamma_{l,g}\sigma^2/\varepsilon$ as obtained by various theoretical methods for Lennard-Jones fluids with experimental data (EXPT) for argon ($\varepsilon/k_B=119.8$ K, $\sigma=3.405$ Å) an xenon ($\varepsilon/k_B=229$ K, $\sigma=4.055$ Å), which practically coincide as a function of $\tau=1-T/T_c$. DFT 1 corresponds to a density-functional theory based on $g^{(2)}=1$ (see the main text), DFT 2 is the density-functional theory used in this paper for $m^*=0$, and DFT 3 the one employed by Ebner, Saam, and Stroud [29]. PT denotes the perturbation theory of Toxvaerd [30]. The simulation data stem from Liu [31] (SIM 1) and Salomons and Mareschal [32] (SIM 2). The experimental data are taken from Refs. [33] and [34].

C. Principle of corresponding states

The grand canonical potential Ω of a Stockmayer fluid at liquid-vapor coexistence within a volume V and with an interface area A depends on V, A, T, ε, σ, and m. In general it has the following form:

$$\Omega=V\frac{\varepsilon}{\sigma^3}\omega^*(T^*,m^*)+A\frac{\varepsilon}{\sigma^2}\gamma^*(T^*,m^*)\ . \tag{5.1}$$

Thus the thermodynamic properties of the bulk and the interface, respectively, for all Stockmayer fluids are determined by the dimensionless functions ω^* and γ^* of the two dimensionless variables $T^*=k_BT/\varepsilon$ and $m^*=m/(\sigma^3\varepsilon)^{1/2}$. This implies that various Lennard-Jones fluids, i.e., $m^*=0$, can be described by a single function $\omega^*_{LJ}(T^*)=\omega^*(T^*,m^*=0)$ of one argument. Traditionally this has been called the principle of corresponding states (see, e.g., Ref. [35]). In this sense the additional dependence on m^* for dipolar fluids represents a deviation from the principle of corresponding states [35]. However, in the bulk and at high temperatures these deviations approximately can be expressed in terms of $\omega^*_{LJ}(T^*)$ after replacing ε and σ by effective, temperature-dependent quantities ε_e and σ_e. For small m^* the Stockmayer fluid can be described by an effective pair potential [see Ref. [35] and Eqs. (3.12) and (3.13) in Ref. [4]]:

$$w_e(r)=4\varepsilon\left[\left(\frac{\sigma}{r}\right)^{12}-\left(\frac{\sigma}{r}\right)^{6}\right]$$
$$+4\varepsilon\left[\frac{7T^*}{1800}\left(\frac{m^*}{\sqrt{T^*}}\right)^{8}\left(\frac{\sigma}{r}\right)^{12}-\frac{T^*}{12}\left(\frac{m^*}{\sqrt{T^*}}\right)^{4}\left(\frac{\sigma}{r}\right)^{6}-\frac{163T^*}{396\,940}\left(\frac{m^*}{\sqrt{T^*}}\right)^{12}\left(\frac{\sigma}{r}\right)^{18}\right]+\cdots$$
$$=4\varepsilon_e\left[\left(\frac{\sigma_e}{r}\right)^{12}-\left(\frac{\sigma_e}{r}\right)^{6}\right]+O\left[T^*\left(\frac{m^*}{\sqrt{T^*}}\right)^{12}\right], \tag{5.2}$$

with

$$\frac{\varepsilon_e}{\varepsilon}=1+\frac{T^*}{6}\left(\frac{m^*}{\sqrt{T^*}}\right)^{4}+\left(\frac{T^{*2}}{144}-\frac{7T^*}{1800}\right)\left(\frac{m^*}{\sqrt{T^*}}\right)^{8}+O(m^{*12}), \tag{5.3}$$

$$\frac{\sigma_e}{\sigma}=1-\frac{T^*}{72}\left(\frac{m^*}{\sqrt{T^*}}\right)^{4}+\left(\frac{7T^{*2}}{10\,368}+\frac{7T^*}{10\,800}\right)\left(\frac{m^*}{\sqrt{T^*}}\right)^{8}+O(m^{*12}), \tag{5.4}$$

and for $T_e^*=k_BT/\varepsilon_e$

$$\frac{T_e^*}{T^*}=1-\frac{T^*}{6}\left(\frac{m^*}{\sqrt{T^*}}\right)^{4}+\left(\frac{T^{*2}}{48}+\frac{7T^*}{1800}\right)\left(\frac{m^*}{\sqrt{T^*}}\right)^{8}+O(m^{*12}). \tag{5.5}$$

This implies that for small $m^*/\sqrt{T^*}$ the grand-canonical potential of a Stockmayer fluid at liquid-gas coexistence can be expressed in terms of the corresponding function of pure Lennard-Jones fluids:

$$\Omega/V=\frac{\varepsilon}{\sigma^3}\omega^*(T^*,m^*)$$
$$=\frac{\varepsilon_e}{\sigma_e^3}\omega^*_{\mathrm{LJ}}(T_e^*)+O(m^{*12}). \tag{5.6}$$

Note that Cook and Rowlinson [35] have called this generalized form a deviation from the principle of corresponding states (as compared with Lennard-Jones liquids). However, we would like to reserve the expression of deviation from the principle of corresponding states to strongly dipolar liquids for which the higher-order terms in Eqs. (5.2)–(5.6) become important. In those cases the effective isotropic interaction of a Stockmayer fluid has no longer the *form* of an effective Lennard-Jones potential so that a mapping onto a corresponding effective Lennard-Jones fluid is no longer possible.

Whereas our approach keeps terms of *all* orders in m^*, the analyses of both Teixeira and Telo da Gama [17] and Yang *et al.* [9,19] keep only—albeit different—terms proportional to m^{*4}. Both groups of authors use as the isotropic part of their pair potential $w(r)=-4\varepsilon\Theta(r-\sigma)(\sigma/r)^6$ with a temperature-independent hard-core diameter σ. Therefore their corresponding effective interaction has the identical form as $w(r)$ with the *only* difference that ε is replaced by ε_e. Consequently, within their model all bulk properties of various Stockmayer fluids can be mapped onto those of a corresponding pure Lennard-Jones fluid by simply rescaling the temperature; the latter can be accomplished by introducing the reduced temperature $\tau=1-T/T_c$. The inclusion of higher-order terms spoils this property. We test their relevance for the water model studied by Yang *et al.* [9,19]. With $\sigma=2.95$ Å, $\varepsilon=1.0777\times10^{-14}$ erg, $m=2.1773\times10^{-18}\sqrt{\text{dyn}}$ cm, $T_c=604.97$ K, and $T_t=273.15$ K one finds at T_c, $\varepsilon_e/\varepsilon=1+6.31+9.24$, $\sigma_e/\sigma=1-0.53+1.09$, and $T_e^*/T^*=1-6.31+30.61$ whereas at T_t one has $\varepsilon_e/\varepsilon=1+13.99+41.11$, $\sigma_e/\sigma=1-1.17+6.06$, and $T_e^*/T^*=1-13.99+154.64$; the order of the various terms corresponds to the one in Eqs. (5.3)–(5.5). Although Yang *et al.* used different and probably more accurate first-order terms, we take the above numbers as indications that for a quantitative description of the water interface the influence of the higher-order terms can be important.

The construction of an effective isotropic pair potential for Stockmayer fluids requires a homogeneous and isotropic liquid. Therefore one cannot expect that the above principle of corresponding states can be generalized to interfacial properties: e.g., such a potential would not lead to an orientational profile. Nonetheless Teixeira and Telo da Gama [17] observed that within their approach the surface tension $\gamma^*_{l,g}$ as a function of $\tau=1-T/T_c(m)$ is nearly independent of m^*, which would indicate a principle of corresponding states even for the surface tension and not only for the bulk. However, Fig. 12 shows that this is only the case for small m^* and at high temperatures. In general we could not find a principle of corresponding states for interfacial properties. However, an indication for a different kind of correspondence principle is provided by Fig. 11.

VI. SUMMARY

Based on the density-functional theory developed in Ref. [4], which implemented a technique put forward by

Blum and Torruella [36], we have obtained the following main results concerning the thermal and structural properties of the intrinsic liquid-vapor interface of a Stockmayer fluid consisting of particles with Lennard-Jones and dipolar interactions.

(i) For small dipole moments m the value of T_c increases proportional to m^4 [Eq. (3.1) and Fig. 1].

(ii) Figures 2 and 3 show the dependence of the density profile $\rho(z)$ and of the profile of the orientational order $\alpha_2(z)$, respectively, on the dipole strength; the latter is proportional to m^4 [Eq. (3.2) and Fig. 4].

(iii) Figures 5 and 6 document the temperature dependence of $\rho(z)$ and its scaling behavior [Eq. (3.6)].

(iv) For $\tau=1-T/T_c\to 0$ the width of the orientational profile diverges $\sim\tau^{-\nu}$ [Eq. (3.12)] whereas the degree of the orientational order vanishes $\sim\tau^{\beta+2\nu}$ [Eq. (3.14)]; see Figs. 7 and 8.

(v) For $\tau\to 0$, $\alpha_2(z)$ also attains a scaling form [Eq. (3.15) and Fig. 9]. The main qualitative feature of $\alpha_2(z)$ has a simple physical interpretation [Eq. (3.16)].

(vi) The dependence of the total surface tension $\gamma_{l,g}$ on the strength of the dipoles and on temperature is shown in Figs. 10 and 12; for small dipole moments there is an approximate correspondence principle (Fig. 11).

(vii) Whereas the total surface tension vanishes as $\gamma_{l,g}(\tau\to 0)\sim\tau^{(d-1)\nu}$ (Fig. 12), the anisotropic contribution to the surface tension vanishes $\sim\tau^{2\beta+(d-1)\nu}$ [Eq. (4.4) and Figs. 14 and 15)] and $\sim m^8$ [Eq. (4.3) and Fig. 13]. The anisotropic contribution is negative, but much smaller than $\gamma_{l,g}$.

(viii) Section V contains a detailed discussion of our results for the density and orientational profiles (Sec. V A) as well as for the surface tension (Sec. V B) and compares them critically with previous results in the literature. There are experimental systems with strong dipole moments for which our approach is quantitatively well suited because it is not a truncated perturbation theory in powers of m^2.

(ix) The principle of corresponding states for dipolar systems is discussed in Sec. V C.

ACKNOWLEDGMENTS

It is a pleasure to thank B. Groh for important hints and very fruitful and valuable assistance. We also would like to thank W. Koch and M. Krech for helpful discussions and A. Haase for his computer graphics program as well as for pertinent advice concerning the layout of the figures.

APPENDIX A: ANALYTIC STRUCTURE OF THE EULER-LAGRANGE EQUATIONS

The Euler-Lagrange equations given in Eqs. (2.15) and (2.16) lead to the equilibrium distributions $\rho(z)$ and $\alpha_2(z)$. Up to the temperature-dependent hard-sphere diameter [Eq. (2.10)] the function $\mu_{\rm HS}(z)$ is known analytically [see Eq. (2.9)]. The value $\mu_0(T)$ of the chemical potential at liquid-vapor coexistence is determined numerically by studying the bulk free energy [4]. Thus the only remaining problem consists in deriving explicit expressions for the coefficients $p_0(z)$ and $p_2(z)$. From Eqs. (4.28)–(4.30), (B27), and (B48)–(B52) in Ref. [4] we have

$$p_0(z)=\int_{-\infty}^{\infty}dz'\rho(z')[\tfrac{1}{2}w_{000}(z'-z)+\alpha_2(z')w_{022}(z'-z)] \tag{A1}$$

and

$$p_2(z)=\int_{-\infty}^{\infty}dz'\rho(z')\{\tfrac{1}{2}w_{202}(z'-z)+\alpha_2(z')[w_{220}(z'-z)+w_{222}(z'-z)+w_{224}(z'-z)]\}\ , \tag{A2}$$

with

$$w_{l_1l_2l}(z)=-\frac{1}{\beta}\frac{1}{\sqrt{4\pi}}\left[\frac{(2l_1+1)(2l+1)}{(2l_2+1)}\right]^{1/2}C(l_1l_2l,000)\times\int_{|z|}^{\infty}dr_{12}r_{12}\Theta(r_{12}-\sigma)\hat{f}_{l_1l_2l}(r_{12})\mathcal{P}_l\left[\frac{z}{r_{12}}\right]. \tag{A3}$$

The values of the Clebsch-Gordon coefficients $C(l_1l_2l,000)$ are given in Sec. IV B of Ref. [4]. The expansion coefficients of the Mayer functions are

$$\hat{f}_{000}(r_{12})=(4\pi)^{3/2}\left[-1+e^{-\beta w_{\rm LJ}(r_{12})}\int_0^1 dx\, i_0[Zh(x)]\right], \tag{A4}$$

$$\hat{f}_{022}(r_{12})=\hat{f}_{202}(r_{12})=2\pi\sqrt{\pi}\,e^{-\beta w_{\rm LJ}(r_{12})}\left[\int_0^1 dx\frac{9x^4+12x^2-1}{1+3x^2}\mathcal{T}(Zh(x))-\int_0^1 dx\left[i_0(Zh(x))-3x^2\frac{3}{Zh(x)}i_1(Zh(x))\right]\right], \tag{A5}$$

$$\hat{f}_{220}(r_{12})=4\pi\sqrt{\pi}\sqrt{5}\,e^{-\beta w_{\rm LJ}(r_{12})}\int_0^1 dx\frac{27x^4-21x^2+2}{1+3x^2}\mathcal{T}(Zh(x))\ , \tag{A6}$$

$$\hat{f}_{222}(r_{12})=4\pi\left[\frac{10\pi}{7}\right]^{1/2}e^{-\beta w_{\rm LJ}(r_{12})}\int_0^1 dx\frac{-18x^4+9x^2+1}{1+3x^2}\mathcal{T}(Zh(x))\ , \tag{A7}$$

and

$$\hat{f}_{224}(r_{12})=10\pi\left[\frac{\pi}{70}\right]^{1/2}e^{-\beta w_{\mathrm{LJ}}(r_{12})}\times\int_0^1 dx\frac{23x^4+6x^2+3}{1+3x^2}\mathcal{T}(Zh(x))\ . \tag{A8}$$

The strength m of the dipole moment enters via the dimensionless parameter $Z=\beta m^2/r_{12}^3$. The function $h(x)$ is defined as $h(x)=(1+3x^2)^{1/2}$. The modified spherical Bessel functions $i_0(y)$ and $i_1(y)$ and $\mathcal{T}(y)=i_0(y)-(3/y)i_1(y)$ have the following series expansions:

$$i_0(y)=\sum_{k=0}^{\infty}\frac{y^{2k}}{(2k+1)!}\ , \tag{A9}$$

$$i_1(y)=\sum_{k=0}^{\infty}\left[\frac{1}{(2k)!}-\frac{1}{(2k+1)!}\right]y^{2k-1}\ , \tag{A10}$$

and

$$\mathcal{T}(y)=\sum_{k=1}^{\infty}\left[\frac{1}{(2k+1)!}-\frac{3}{(2k+2)!}+\frac{3}{(2k+3)!}\right]y^{2k}\ . \tag{A11}$$

If these expansions are inserted into Eqs. (A4)–(A8) one obtains

$$\hat{f}_{l_1l_2l}(r_{12})=F_{l_1l_2l}\,e^{-\beta w_{\mathrm{LJ}}(r_{12})}\sum_{k=1}^{\infty}\alpha_{l_1l_2l}^{(k)}Z^{2k}-(4\pi)^{3/2}\delta_{0,l_1+l_2+l_3}\ , \tag{A12}$$

where $F_{000}=(4\pi)^{3/2}$, $F_{202}=F_{022}=2\pi\sqrt{\pi}$, $F_{220}=4\pi\sqrt{5\pi}$, $F_{222}=4\pi(10\pi/7)^{1/2}$, and $F_{224}=10\pi(\pi/70)^{1/2}$. The numbers $a_{l_1l_2l}^{(k)}$ are determined by

$$a_{000}^{(k)}=\frac{1}{(2k+1)!}\sum_{j=0}^{k}\begin{bmatrix}k\\j\end{bmatrix}\frac{3^j}{2j+1}\ , \tag{A13}$$

$$a_{202}^{(k)}=-\frac{1}{(2k+1)!}\times\sum_{j=0}^{k}\begin{bmatrix}k\\j\end{bmatrix}3^j\left[\frac{1}{2j+1}-\frac{9}{(2k+3)(2j+3)}\right]+\frac{4k(k+1)}{(2k+3)!}I_{202}^{(k)}\ , \tag{A14}$$

$$a_{202}^{(k)}=\frac{4k(k+1)}{(2k+3)!}I_{220}^{(k)}\ , \tag{A15}$$

$$a_{222}^{(k)}=\frac{4k(k+1)}{(2k+3)!}I_{222}^{(k)}\ , \tag{A16}$$

and

$$a_{224}^{(k)}=\frac{4k(k+1)}{(2k+3)!}I_{224}^{(k)}\ . \tag{A17}$$

The numbers $I_{l_1l_2l}^{(k)}$ are defined as

$$I_{202}^{(k)}=\int_0^1 dx(9x^4+12x^2-1)(1+3x^2)^{k-1}\ , \tag{A18}$$

$$I_{220}^{(k)}=\int_0^1 dx(27x^4-21x^2+2)(1+3x^2)^{k-1}\ , \tag{A19}$$

$$I_{222}^{(k)}=\int_0^1 dx(-18x^4+9x^2+1)(1+3x^2)^{k-1}\ , \tag{A20}$$

and

$$I_{224}^{(k)}=\int_0^1 dx(23x^4+6x^2+3)(1+3x^2)^{k-1}\ ; \tag{A21}$$

they have been determined for $k\le 15$ by using the computer program MATHEMATICA. In the next step Eq. (A12) is inserted into Eq. (A3), which in turn is used in Eqs. (A1) and (A2). This leads directly to Eq. (2.18) with the following expressions for the functions $w_{mn}(z)$:

$$w_{00}(z)=-\frac{\beta}{2\pi}w_{000}(z)=2\int_{|z|}^{\infty}dr_{12}r_{12}\Theta(r_{12}-\sigma)\times\left[-1+e^{-\beta w_{\mathrm{LJ}}(r_{12})}\sum_{k=0}^{\infty}a_{000}^{(k)}Z^{2k}\right]\ , \tag{A22}$$

$$w_{02}(z)=-\frac{\beta}{\pi}w_{022}(z)=\int_{|z|}^{\infty}dr_{12}r_{12}\Theta(r_{12}-\sigma)e^{-\beta w_{\mathrm{LJ}}(r_{12})}\times\sum_{k=1}^{\infty}a_{202}^{(k)}\mathcal{P}_2\left[\frac{z}{r_{12}}\right]Z^{2k}\ , \tag{A23}$$

$$w_{20}(z)=-\frac{\beta}{2\pi}w_{202}(z)=\int_{|z|}^{\infty}dr_{12}r_{12}\Theta(r_{12}-\sigma)e^{-\beta w_{\mathrm{LJ}}(r_{12})}\times\sum_{k=1}^{\infty}\frac{5}{2}a_{202}^{(k)}\mathcal{P}_2\left[\frac{z}{r_{12}}\right]Z^{2k}\ , \tag{A24}$$

and

$$w_{22}(z)=-\frac{\beta}{\pi}\sum_{l=0,2,4}w_{22l}(z)=\int_{|z|}^{\infty}dr_{12}r_{12}\Theta(r_{12}-\sigma)e^{-\beta w_{\mathrm{LJ}}(r_{12})}\times\sum_{k=1}^{\infty}\left[2a_{220}^{(k)}-\frac{20}{7}a_{222}^{(k)}\mathcal{P}_2\left[\frac{z}{r_{12}}\right]+\frac{9}{7}a_{224}^{(k)}\mathcal{P}_4\left[\frac{z}{r_{12}}\right]\right]Z^{2k}\ . \tag{A25}$$

In practice the sums in Eqs. (A22)–(A25) have been truncated for $k>15$, which causes an error of less than 10^{-6} for $Z\le 4$. Together with Eqs. (A1) and (A2) one finally obtains Eq. (2.18).

Equations (A3) and (A22)–(A25) show that the presence of the Heaviside function in the integrand of Eq. (A3) leads to a discontinuity of the derivative of $w_{mn}(z)$ at $z=\sigma$. This cusplike singularity of the functions w_{mn} is displayed in Fig. 17. In order to avoid numerical difficulties induced by this cusp the integration over z' in Eq. (2.18) is split into three parts: one for $-\infty<z'\le z-\sigma$, one for $z-\sigma\le z'\le z+\sigma$, and one for $z+\sigma\le z'<\infty$. The accuracy of the integration procedure has been tested successfully by studying to which extent the relation

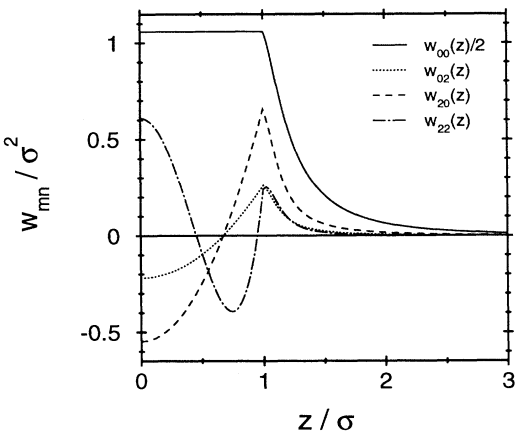

FIG. 17. The functions w_{mn} defined by Eqs. (A22)–(A25) in units of σ^2 for $T^*=k_BT/\varepsilon=1.3$ and $m^*=m/\sqrt{\varepsilon\sigma^3}=1.5$. These functions have a cusplike singularity at $z=\sigma$. Note that $\int_0^\infty dz\, w_{20}(z)=0$ [see Eq. (A26)].

$$\int_0^\infty dz\, w_{20}(z)=0 \tag{A26}$$

is fulfilled. Equation (A26) follows from the observation that Eqs. (2.15) and (2.16) are solved by the bulk solution $\rho(z)=$const and $\alpha_2(z)\equiv 0$. According to Eq. (2.16) this implies $p_2(z)\equiv 0$ in that case and thus $\int_0^\infty dz\, w_{202}(z)=0$ [see Eqs. (A2) and (A24)].

Finally we want to mention that the numerical procedure for solving Eqs. (2.15) and (2.16) can be facilitated since the explicit integral displayed in these two equations can be expressed in terms of the error function $\mathrm{erf}(x)=(2/\sqrt{\pi})\int_0^x dt\, e^{-t^2}$ and Dawson's integral $F(x)=e^{-x^2}\int_0^x dt\, e^{t^2}$ [37]:

$$\mu_{\mathrm{HS}}(z)=\mu_0(T)+\frac{1}{\beta}[\hat{p}_0(z)-\tfrac{1}{2}\hat{p}_2(z)+\ln e(z)] \tag{A27}$$

and

$$\alpha_2(z)=\frac{5}{4}\left[-\frac{1}{\hat{p}_2(z)}-f(z)-1\right], \tag{A28}$$

where

$$e(z)=\begin{cases}\left[\dfrac{\pi}{6|\hat{p}_2(z)|}\right]^{1/2}\mathrm{erf}[\sqrt{\tfrac{3}{2}|\hat{p}_2(z)|}]\,, & \hat{p}_2(z)<0\\ 1\,, & \hat{p}_2(z)=0\\ \left[\dfrac{2}{3\hat{p}_2(z)}\right]^{1/2}e^{(3/2)\hat{p}_2(z)}F(\sqrt{\tfrac{3}{2}\hat{p}_2(z)})\,, & \hat{p}_2(z)>0\end{cases} \tag{A29}$$

and

$$f(z)=\begin{cases}\sqrt{6}e^{(3/2)\hat{p}_2(z)}\{\sqrt{\pi|\hat{p}_2(z)|}\,\mathrm{erf}[\sqrt{\tfrac{3}{2}|\hat{p}_2(z)|}]\}^{-1}\,, & \hat{p}_2(z)<0\\ -1-\dfrac{1}{\hat{p}_2(z)}\,, & \hat{p}_2(z)\to 0\\ -3[\sqrt{6\hat{p}_2(z)}F(\sqrt{\tfrac{3}{2}\hat{p}_2(z)})]^{-1}\,, & \hat{p}_2(z)>0\,.\end{cases} \tag{A30}$$

Here we have introduced the dimensionless quantities

$$\hat{p}_m(z)=-\beta p_m(z)\,,\quad m=0,2\,. \tag{A31}$$

APPENDIX B: NUMERICAL SOLUTION OF THE EULER-LAGRANGE EQUATIONS

Since standard approaches for solving Eqs. (A27) and (A28) lead either to a poor numerical accuracy or to unphysical oscillatory structures in $\alpha_2(z)$, in the following we describe our numerical method for obtaining reliable results for $\rho(z)$ and $\alpha_2(z)$.

For the size L of the system we have chosen $L=60\sigma$, i.e., $-30\le z/\sigma\le 30$ and a grid of $N=2401$ mesh points, i.e., $\Delta z=z_{i+1}-z_i=0.025\sigma$. Outside $|z|\le L/2$ we adopt the bulk properties for both $\rho(z)$ and $\alpha_2(z)$: $\rho(z<-L/2)=\rho_l$, $\rho(z>L/2)=\rho_g$, and $\alpha_2(|z|>L/2)=0$. Nonetheless, these latter values lead to asymptotic contributions to the coefficients $\hat{p}_m(z)$ [see Eqs. (2.18) and (A31)],

$$\hat{p}_m^{\mathrm{asy}}(z)=\pi\rho_l\int_{-\infty}^{-L/2}dz'w_{m0}(z'-z)+\pi\rho_g\int_{L/2}^{\infty}dz'w_{m0}(z'-z)\,, \tag{B1}$$

while for $|z|\le L/2$, Eq. (2.18) is applied with the z' integration confined to $|z|\le L/2$.

The discretized versions of Eqs. (2.15) and (2.16) have the form $(i,j=1,\ldots,N)$

$$\mu_{\rm HS}[\rho^{(n+1)}(z_i)]=\mathcal{A}(\{\rho^{(n)}(z_j)\},\{\alpha_2^{(n)}(z_j)\},z_i) \tag{B2}$$

and

$$\alpha_2^{(n+1)}(z_i)=\mathcal{B}(\{\rho^{(n)}(z_j)\},\{\alpha_2^{(n)}(z_j)\},z_i)\ . \tag{B3}$$

Here we have already implemented the following iteration procedure: on the right-hand sides of Eqs. (2.15) and (2.16) initial guesses $\rho^{(0)}(z)$ and $\alpha_2^{(0)}(z)$ are inserted which, according to these equations, lead to certain expressions on the left-hand sides which are denoted by $\mu_{\rm HS}[\rho^{(1)}(z)]$ and $\alpha_2^{(1)}(z)$, respectively. Since $\mu_{\rm HS}(\rho)$ is a monotonous function of ρ [see Eqs. (2.9) and (2.17)], $\rho^{(1)}(z)$ follows uniquely from $\mu_{\rm HS}[\rho^{(1)}(z)]$. $\rho^{(1)}(z)$ and $\alpha^{(1)}(z)$ are now reinserted into the right-hand side leading to $\rho^{(2)}(z)$ and $\alpha_2^{(2)}(z)$ etc. We repeated this procedure until we found $|\Delta\rho^{(n)}(z)|=|\rho^{(n)}(z)-\rho^{(n-1)}(z)|\le 10^{-5}G^3$ and $|\Delta\alpha_2^{(n)}(z)|=|\alpha_2^{(n)}(z)-\alpha_2^{(n-1)}(z)|\le 10^{-5}$ for each value $z=z_i$, $i\in\{1,\ldots,N\}$.

However, in order to achieve a regular convergence of the above procedure we had to modify it by using a method of underrelaxation, which can be applied easily because both $\hat{p}_0(z)$ and $\hat{p}_2(z)$ are linear in $\rho(z)$ and $\alpha_2(z)$ [see Eqs. (2.18) and (A31)]. According to that method the variations $\Delta\rho^{(n)}(z)$ and $\Delta\alpha_2^{(n)}(z)$ from one iteration step to the next are controlled by two relaxation parameters $\eta_1^{(n)}$ and $\eta_2^{(n)}$:

$$\begin{aligned}\hat{p}_m^{(n)}(z)=&\pi\int_{-L/2}^{L/2}dz'\rho^{(n-1)}(z')[w_{m0}(z'-z)+\alpha_2^{(n-1)}(z')w_{m2}(z'-z)]\\&+\frac{\pi}{1+1/\eta_1^{(n)}}\int_{-L/2}^{L/2}dz'\Delta\rho^{(n)}(z')[w_{m0}(z'-z)+\alpha_2^{(n-1)}(z')w_{m2}(z'-z)]\\&+\frac{\pi}{1+1/\eta_2^{(n)}}\int_{-L/2}^{L/2}dz'\rho^{(n)}(z')\Delta\alpha_2^{(n)}(z')w_{m2}(z'-z)+\hat{p}_m^{\rm asy}(z)\ .\end{aligned} \tag{B4}$$

$\hat{p}_m^{(n)}(z)$, $m=0$, 2, are used on the right-hand side of Eqs. (2.15) and (2.16) in order to obtain $\rho^{(n+1)}(z)$ and $\alpha_2^{(n+1)}(z)$ from the corresponding left-hand side. The original iteration procedure is recovered for $\eta_1^{(n)}=\eta_2^{(n)}=\infty$. We decreased $\eta_1^{(n)}$ and $\eta_2^{(n)}$ from 100 to 1 with increasing index n of the iteration. With this method we obtained a regular and stable convergence of the iteration which also turned out to be very robust with respect to various choices for the initial guesses.

APPENDIX C: EXPLICIT EXPRESSIONS FOR THE SURFACE TENSION

The surface tension consists of three distinct contributions [see Eq. (4.1)] whose general formulas are given by Eqs. (4.34)–(4.37) in Ref. [4]. By taking into account that in our present approach the angular dependence of α is truncated after $l=2$ [see Eq. (2.13)] these three contributions can be expressed explicitly in terms of the functions $w_{mn}(z)$ defined in Eqs. (A22)–(A25), $\alpha_2(z)$, and $\delta\rho(z)=\rho(z)-\rho_{\rm SK}(z)$, where $\rho_{\rm SK}(z)=\rho_l-\Delta\rho\Theta(z)$ with $\Delta\rho=\rho_l-\rho_g$ is the sharp-kink (SK) density profile. (Note that in order to avoid confusion with the hard-core diameter σ, in this paper the surface tension is denoted by $\gamma_{l,g}$ instead of $\sigma_{l,g}$ as in Ref. [4].) For $\gamma_{l,g}^{(\rho)}$ one finds [see Eq. (4.35) in Ref. [4] and Eq. (A22)]:

$$\begin{aligned}\gamma_{lg}^{(\rho)}=\lim_{L\to\infty}\Bigg[&\int_{-L/2}^{L/2}dz\{f_{\rm ref}^{\rm HS}[\rho(z),T]-f_{\rm ref}^{\rm HS}[\rho_{\rm SK}(z),T]+[w_0\rho_{\rm SK}(z)-\mu_0(T)]\delta\rho(z)\}\\&-\pi k_BT\Bigg\{\frac{1}{2}\mathcal{I}_1\left[\frac{L}{2}\right]+\Delta\rho\left[\mathcal{I}_2\left[-\frac{L}{2},0;\frac{L}{2}\right]+\mathcal{I}_2\left[-\infty,-\frac{L}{2};\frac{L}{2}\right]-\mathcal{I}_3\left[0,\frac{L}{2};\frac{L}{2}\right]-\mathcal{I}_3\left[\frac{L}{2},\infty;\frac{L}{2}\right]\right]\\&-\frac{1}{2}(\Delta\rho)^2\left[\mathcal{I}_4\left[-\frac{L}{2},0;\frac{L}{2}\right]+2\mathcal{I}_4\left[-\infty,\frac{L}{2};\frac{L}{2}\right]+\mathcal{I}_5\left[\infty,\frac{L}{2}\right]\right]\Bigg\}\Bigg]\end{aligned} \tag{C1}$$

with

$$w_0=-2\pi k_BT\int_0^\infty dy\ w_{00}(y)\ , \tag{C2}$$

$$\mathcal{I}_1\left[\frac{L}{2}\right]=\int_{-L/2}^{L/2}dz\ \delta\rho(z)\int_{-L/2}^{L/2}dz'\delta\rho(z')w_{00}(z-z')\ , \tag{C3}$$

$$\mathcal{I}_2\left[a,b;\frac{L}{2}\right]=\int_a^b dz\int_0^{L/2}dz'\delta\rho(z')w_{00}(z-z')\ , \tag{C4}$$

$$\mathcal{I}_3\left[a,b;\frac{L}{2}\right]=\int_a^b dz\int_{-L/2}^{0}dz'\delta\rho(z')w_{00}(z-z')\ , \tag{C5}$$

$$\mathcal{I}_4\left[a,b;\frac{L}{2}\right]=\int_a^b dz\int_0^{L/2}dz' w_{00}(z-z')\ , \tag{C6}$$

and

$$\mathcal{I}_5\left[\infty,\frac{L}{2}\right]=\int_{-\infty}^{-L/2}dz\int_{L/2}^{\infty}dz' w_{00}(z-z')\ . \tag{C7}$$

In the limit $L\to\infty$ the asymptotic terms $\mathcal{I}_2(-\infty,-L/2;L/2)$, $\mathcal{I}_3(L/2,\infty;L/2)$, $\mathcal{I}_4(-\infty,-L/2;L/2)$, and $\mathcal{I}_5(\infty,L/2)$ vanish and thus they are redundant in Eq. (C1). However, since the limit $L\to\infty$ has to be performed by extrapolating numerical data obtained from finite system sizes, the particular representation given by Eq. (C1) has proven to be efficient for that purpose.

For the purely entropic contribution to the surface tension we obtain from Eq. (4.36) in Ref. [4]:

$$\gamma_{l,g}^{(\mathcal{S})}=\frac{1}{\beta}\lim_{L\to\infty}\int_{-L/2}^{L/2}dz\,\rho(z)\{\ln[1+2\alpha_2(z)]+\tfrac{2}{3}[\alpha_2(z)-2]+\tfrac{4}{3}[1-\alpha_2(z)]\sqrt{|a(z)|}f_{\pm}[|a(z)|^{-1/2}]\}\ , \tag{C8}$$

with

$$a(z)=\frac{1}{3}\left[\frac{1}{\alpha_2(z)}-1\right]\ , \tag{C9}$$

$$f_+(y)=\text{arctanh}y\ ,\quad \alpha_2(z)>0\ , \tag{C10}$$

and

$$f_-(y)=\tfrac{1}{2}\ln\left[\frac{1+y}{1-y}\right]=\text{arctanh}y\ ,\quad \alpha_2(z)\le 0\ . \tag{C11}$$

Finally the explicit expression for the anisotropic contribution to the surface tension follows from Eq. (4.37) in Ref. [4] [see Eqs. (A23) and (A25)]:

$$\begin{aligned}\sum_{\Lambda[\neq(000)]}\gamma_{l,g}^{(\Lambda)}=-\pi k_B T\lim_{L\to\infty}\Bigg\{&\int_{-L/2}^{L/2}dz\,\rho(z)\int_{-L/2}^{L/2}dz'\rho(z')\alpha_2(z')w_{02}(z-z')\\&+\tfrac{1}{5}\int_{-L/2}^{L/2}dz\,\rho(z)\alpha_2(z)\int_{-L/2}^{L/2}dz'\,\rho(z')\alpha_2(z')w_{22}(z-z')\\&+\rho_l\int_{-\infty}^{-L/2}dz\int_{-L/2}^{L/2}dz'\rho(z')\alpha_2(z')w_{02}(z-z')\\&+\rho_g\int_{L/2}^{\infty}dz\int_{-L/2}^{L/2}dz'\rho(z')\alpha_2(z')w_{02}(z-z')\Bigg\}\ .\end{aligned} \tag{C12}$$

The last two terms in Eq. (C12) arise due to $\rho(z<-L/2)=\rho_l$ and $\rho(z>L/2)=\rho_g$ (see Appendix B); they play a role similar to the asymptotic terms in Eq. (C1). Equations (C1), (C8), and (C12) are the basis for the numerical calculation of the liquid-vapor surface tension.

[1] D. E. Sullivan and M. M. Telo da Gama, in *Fluid Interfacial Phenomena,* edited by C. A. Croxton (Wiley, Chichester, 1986), p. 45.

[2] S. Dietrich, in *Phase Transitions and Critical Phenomena,* edited by C. Domb and J. L. Lebowitz (Academic, London, 1988), Vol. 12, p. 1.

[3] *Liquids at Interfaces,* edited by J. Charvolin, J. F. Joanny, and J. Zinn-Justin, Les Houches Summer School Lectures, Session XLVIII (Elsevier, Amsterdam, 1990); see in particular the contributions by R. Evans, P. G. de Gennes, J. Meunier, A. M. Cazabat, M. Schick, and D. Beysens.

[4] P. Frodl and S. Dietrich, Phys. Rev. A **45**, 7330 (1992), and references therein.

[5] N. F. Carnahan and K. E. Starling, J. Chem. Phys. **51**, 635 (1969).

[6] J. A. Barker and D. Henderson, J. Chem. Phys. **47**, 4714 (1967).

[7] S. Dietrich and M. Napiórkowski, Phys. Rev. A **43**, 1861 (1991).

[8] S. M. Thompson, K. E. Gubbins, and J. M. Haile, J. Chem. Phys. **75**, 1325 (1981).

[9] B. Yang, D. E. Sullivan, B. Tjipto-Margo, and C. G. Gray, Mol. Phys. **76**, 709 (1992).

[10] J. S. Rowlinson and B. Widom, *Molecular Theory of Capillarity* (Clarendon, Oxford, 1982).

[11] B. Groh (private communication).

[12] K. E. Gubbins, in *Fluid Interfacial Phenomena* (Ref. [1]), p. 469.

[13] K. E. Gubbins and S. M. Thompson, Faraday Symp. Chem. Soc. London **16**, 59 (1981).

[14] E. Chacón, P. Tarazona, and G. Navascués, J. Chem. Phys. **79**, 4426 (1983).
[15] J. Eggebrecht, K. E. Gubbins, and S. M. Thompson, J. Chem. Phys. **86**, 2286 (1987).
[16] J. Eggebrecht, S. M. Thompson, and K. E. Gubbins, J. Chem. Phys. **86**, 2299 (1987).
[17] P. I. Teixeira and M. M. Telo da Gama, J. Phys. Condens. Matter **3**, 111 (1991).
[18] P. I. Teixeira, B. S. Almeida, M. M. Telo da Gama, J. A. Rueda, and R. G. Rubio, J. Phys. Chem. **96**, 8488 (1992).
[19] B. Yang, D. E. Sullivan, B. Tjipto-Margo, and C. G. Gray, J. Phys. Condens. Matter **3**, F109 (1991).
[20] J. P. Badiali, J. Chem. Phys. **89**, 2397 (1988).
[21] Q. Zhang, J. P. Badiali, and W. H. Su, J. Chem. Phys. **92**, 4609 (1990); Q. Zhang, J. P. Badiali, and M. L. Rosinberg, J. Mol. Liq. **48**, 129 (1991).
[22] J. P. Badiali and F. Forstmann, Chem. Phys. **141**, 63 (1990).
[23] J. P. Badiali, J. Chem. Phys. **90**, 4401 (1989).
[24] N. I. Lebovka, F. D. Ovcharenko, and V. V. Mank, Dokl. Akad. Nauk SSSR **285**, 392 (1985).
[25] C. G. Gray and K. E. Gubbins, Mol. Phys. **30**, 179 (1975).
[26] J. M. Haile, C. G. Gray, and K. E. Gubbins, J. Chem. Phys. **64**, 2569 (1976).
[27] B. Smit, C. P. Williams, E. M. Hendriks, and S. W. de Leeuw, Mol. Phys. **68**, 765 (1989).
[28] A. Latz and S. Dietrich, Phys. Rev. B **40**, 9204 (1989).
[29] C. Ebner, W. F. Saam, and D. Stroud, Phys. Rev. A **14**, 2264 (1976).
[30] S. Toxvaerd, J. Chem. Phys. **55**, 3116 (1971).
[31] K. S. Liu, J. Chem. Phys. **60**, 4226 (1974).
[32] E. Salomons and M. Mareschal, J. Phys. Condens. Matter **3**, 3645 (1991).
[33] D. Stanfield, Proc. Phys. Soc. London **72**, 854 (1958); some data can be traced back to E. Mathias, H. K. Onnes, and C. A. Crommelin, Comm. Phys. Lab. Univ. Leiden No. 131(a) (1912).
[34] B. L. Smith, P. R. Gardner, and H. C. Parker, J. Chem. Phys. **47**, 1148 (1967).
[35] D. Cook and J. S. Rowlinson, Proc. Soc. London Ser. A **219**, 405 (1953).
[36] L. Blum and A. J. Torruella, J. Chem. Phys. **89**, 4976 (1988).
[37] *Handbook of Mathematical Functions,* edited by M. Abramowitz and I. A. Stegun (Dover, New York, 1970), Chap. 7.